iScience

CellPress
OPEN ACCESS

Review

Recent advances in developing multiscale descriptor approach for the design of oxygen redox electrocatalysts

Dantong Zhang,[1] Qi Zhang,[1] Chao Peng,[1,*] Zhi Long,[1] Guilin Zhuang,[2] Denis Kramer,[3] Sridhar Komarneni,[4] Chunyi Zhi,[5,*] and Dongfeng Xue[1,*]

SUMMARY

Oxygen redox electrocatalysis is the crucial electrode reaction among new-era energy sources. The prerequisite to rationally design an ideal electrocatalyst is accurately identifying the structure-activity relationship based on the so-called descriptors which link the catalytic performance with structural properties. However, the quick discovery of those descriptors remains challenging. In recent, the high-throughput computing and machine learning methods were identified to present great prospects for accelerating the screening of descriptors. That new research paradigm improves cognition in the way of oxygen evolution reaction/oxygen reduction reaction activity descriptor and reinforces the understanding of intrinsic physical and chemical features in the electrocatalytic process from a multiscale perspective. This review summarizes those new research paradigms for screening multiscale descriptors, especially from atomic scale to cluster mesoscale and bulk macroscale. The development of descriptors from traditional intermediate to eigen feature parameters has been addressed which provides guidance for the intelligent design of new energy materials.

INTRODUCTION

Oxygen redox electrochemical reactions, namely the oxygen evolution reaction (OER) and the oxygen reduction reaction (ORR) are the key electrode reactions in the aspect of green energy storage and conversions, for instance, alkaline fuel cells and metal-air batteries (Figure 1A).[1–3] The OER and ORR catalytic activity directly determines the battery performance including energy conversion efficiency, battery charge/discharge rate, and power density. In terms of the reversible OER and ORR reactions in batteries, the single catalyst cannot meet the satisfaction of both reactions. For example, the most active electrocatalyst for OER is RuO_2, showing great electrical and ionic conductivity, while this catalyst is not suitable for ORR because of the too weak O_2 binding ability. The state-of-art electrocatalyst for ORR is Pt, while the formation of Pt oxide film in OER decays the long-term stability. Therefore, rationally designing bifunctional low-cost OER/ORR electrocatalysts satisfying the catalytic performance including activity and long lifetime has attracted much attention. The key to catalyst design is identifying the effective descriptor linking structure and activity to accelerate the cycle of the research and development (R&D) process for quickly screening excellent catalysts from the materials database. However, due to the complicated catalytic process, discovering the effective bifunctional descriptor to meet the electrocatalytic activity and the selectivity remains a challenge.[4–6] The OER and ORR activity was highly dependent on the adsorbed Gibbs free energy of the three key intermediates *OOH, *O, and *OH.[7–9] The classical Sabatier principle exhibits that the superior catalytic performance occurs when interactions between the catalyst and the reactant are of moderate strength exhibited at the top of the Balandine-type "volcano curve". However, there lacks efficient way in correlating the binding strength of the intermediate with the eigen electronic and geometric structure of catalysts, thus generating a barrier to identifying the intrinsic descriptor for the design and synthesis of OER/ORR catalysts.

The era of big data provides an opportunity for the investigation of intrinsic descriptors based on the new paradigms development of high-throughput computing and machine learning (ML) used in materials screening and designing.[12–14] Even though the *d*-band center (ε_d) was verified to have a generally linear correlation with OER/ORR activity in the majority of catalytic systems, the coordination of active sites, size of the

[1]Multiscale Crystal Materials Research Center, Shenzhen Institute of Advanced Technology, Chinese Academy of Sciences, Shenzhen 518055, China

[2]College of Chemical Engineering, Zhejiang University of Technology, 18, Chaowang Road, Hangzhou, Zhejiang Province 310032, China

[3]Helmut-Schmidt-University, University of the Armed Forces, Hamburg 22043, Germany

[4]Materials Research Institute, Materials Research Laboratory, The Pennsylvania State University, University Park, PA 16802, USA

[5]Department of Materials Science and Engineering, City University of Hong Kong, Kowloon, Hong Kong 999077, China

*Correspondence: chao.peng@siat.ac.cn (C.P.), cy.zhi@cityu.edu.hk (C.Z.), df.xue@siat.ac.cn (D.X.)

https://doi.org/10.1016/j.isci.2023.106624

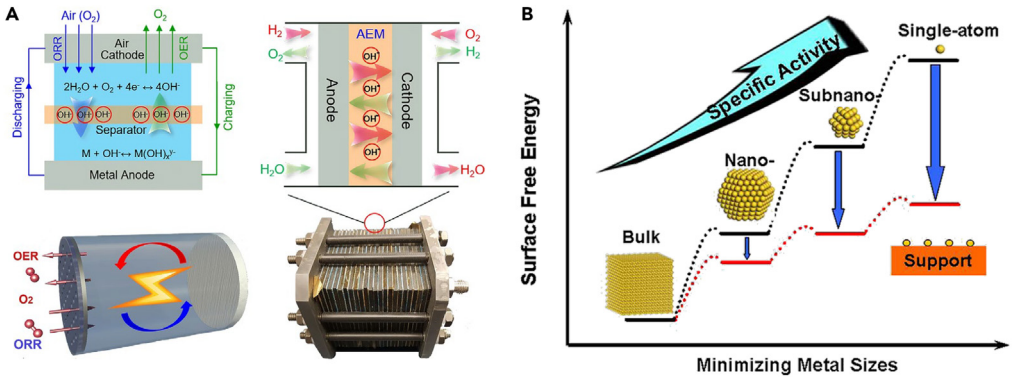

Figure 1. OER/ORR utilization in energy transfer/storage and the diagram of multiscale catalysts

(A) The mechanism diagram of metal-air batteries and regenerative fuel cells. Reproduced with permission from[10] copyright 2022 Springer Nature.

(B) The specific activity and surface energy change of multiscale atomic models with the minimizing metal sizes. Reproduced with permission from[11] copyright 2013 American Chemical Society.

catalyst, and related factors were also found to show impacts.[15–17] Single-atom catalysts are hot-pot materials due to the large specific surface area.[18–20] The overpotential and current density of metal-N-C systems are highly correlated with the N-C coordination environment. The cluster mesoscale material is generally composed of highly active metallic centers and ligands, and its performance not only depends on the *d* electron center but also relates to the geometric structure of the bond length, bond angle, and coordinated ligands.[21,22] The performance of three-dimensional metal oxides is highly correlated with the electron spin state and band center of the metal part.[23] Therefore, finding out the influences of those factors and parameterizing them as descriptors endowing with different importance are crucial to constructing structure-performance relationships for designing highly active and stable OER/ORR catalysts.[24,25]

There are considerable amount of literature published to discuss the descriptors which can be classified into two categories including electronic- and geometric-based descriptors. For the electronic-based descriptors, i.e., ε_d, e_g filling, *p*-band center, transferred charge amount, electronegativity, electron affinity, and ionization potential/energy, have been widely developed. The catalytic performance of transition metal oxides (TMOs) has been found sensitive to electronic orbital. There exist higher exchange current densities and lower Tafel's slope in TMOs with filled t_{2g} orbitals and partially filled e_g orbitals than that in TMOs with partially t_{2g} orbitals and empty e_g orbitals.[26] From a quantitative perspective, the *d*-band theory was thereafter proposed and has been widely applied in heterogeneous catalysis. The ε_d of transition metals (TMs) in a single-atom TMs-N_4-C system was found to be highly sensitive to ligand-effect, strain-effect, and the coordination number of Nitride-Carbon around the active site. The relative position of ε_d and Fermi level can be used as the descriptor to explore the structure-activity relation. Furthermore, the geometric-based descriptor also acts as auxiliary composition to improve the accuracy score of structure-performance prediction. Atomic radius, atomic volume, space group, system symmetry as well as coordination number are the main geometric descriptors, linked to the catalytic properties. The combination of geometric and electronic features often provides a more precise description of the catalyst's performance. Compared to the single-component descriptor of coordinated atomic numbers that reflecting the geometric environment of active centers, the multi-component descriptor including both bond energy, chemical environment, and geometric coordinated atomic number is more precisely to describe the catalytic performance of Pt catalyst and TMOs.[27]

Although the descriptors for catalyst design have achieved great progress, the single descriptor still has inherent limitations to completely describe the properties of the catalyst. In this review, we summarized the development and limitation of benchmark descriptors as well as the application and prospect of multi-feature composite descriptors achieved by ML methods with new insights paid from the atomic microscale to the cluster mesoscale and the bulk macroscale (Figure 1B).[28,29] The descriptor feature importance and correlation to obtain guidelines for interface engineering were addressed. Finally, we discussed the applications and showed the perspective for the development of descriptors to design better heterogeneous catalysts.

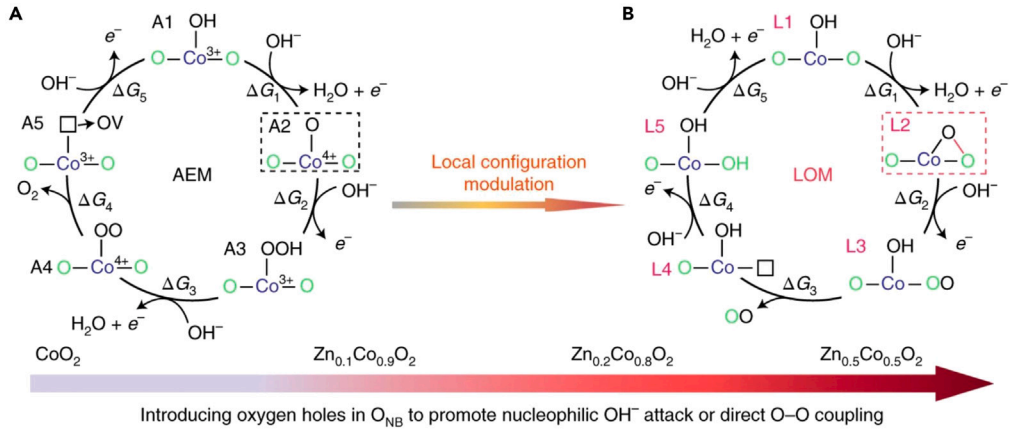

Figure 2. AEM and LOM reaction path in OER

(A) Schematics of adsorbates evolution mechanism.

(B) Schematics of lattice-oxygen participated mechanism. Reproduced with permission from[36] copyright 2019 Springer Nature.

REACTION MECHANISM FOR OER AND ORR

Understanding OER/ORR mechanism is essential to design superior bifunctional oxygen redox electrocatalysts.[30–32] The OER/ORR activity is closely related to the reaction paths and complex oxygen intermediates. Thus, this section provides an overview of the intermediate process and reaction mechanism of the reversible oxygen redox reactions, providing new insight into novel theoretical guidance for designing the optimal bifunctional OER/ORR electrocatalysts.

OER mechanism

OER is an important reaction in alkaline fuel cells and secondary metal-air batteries. However, the unbefitting binding strength and depressed reaction dynamics of oxygenated intermediates on the OER catalyst impose a large inherent overpotential. Currently, IrO_2 and RuO_2 are the mainly commercial and benchmark OER catalyst, but their scarce resources limit further applications. Over the past few years, the OER catalysts were focused on metal oxide,[33] perovskite,[34] and spinel materials.[35] The recognized OER mechanism was based on the adsorbate evolution mechanism (AEM) (Figure 2A) and lattices oxygen oxidation mechanism (LOM) (Figure 2B). There exists highly linear correlation between adsorption Gibbs free energy of three adsorbed intermediates in AEM process, thus causing the minimum theoretical overpotential around 0.37 V.[36] And the restriction of minimum overpotential is removed by the direct O-O coupling between lattice and adsorbed oxygen atoms in LOM process.[37] AEM can be considered as a redox reaction of metal cations, and oxygen generation in alkaline solution is follows Equations 1, 2, 3, and 4, exhibited a four-electron transfer process. (Equation 5)

$$* + OH^- (aq) \rightarrow *OH + e^- \quad \text{(Equation 1)}$$

$$*OH + OH^- (aq) \rightarrow *O + H_2O (l) + e^- \quad \text{(Equation 2)}$$

$$*O + OH^- (aq) \rightarrow *OOH + e^- \quad \text{(Equation 3)}$$

$$*OOH + OH^- (aq) \rightarrow * + O_2 + H_2O + e^- \quad \text{(Equation 4)}$$

$$\text{Overall: } 4OH^- (aq) \rightarrow O_2 (g) + 2H_2O (l) + 4e^- \quad \text{(Equation 5)}$$

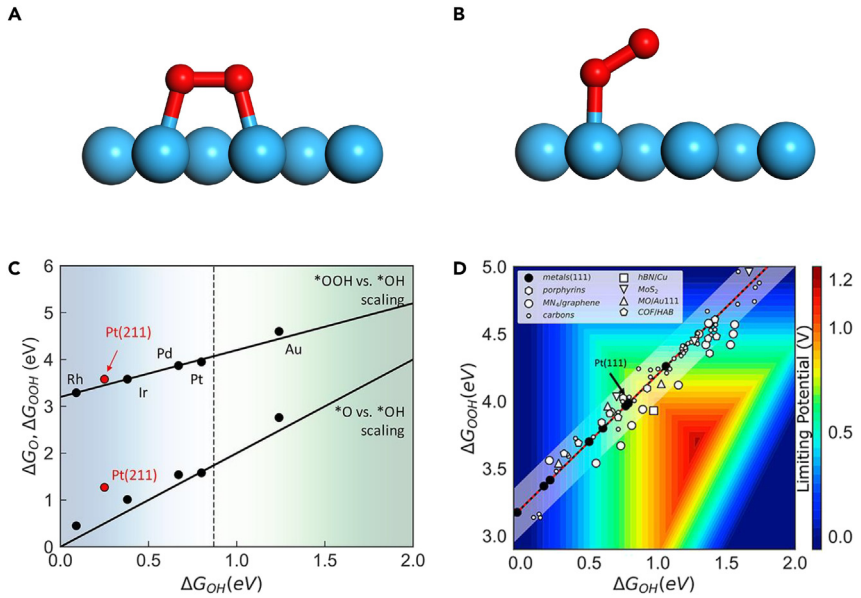

Figure 3. O_2 adsorption configuration and correlation between intermediates and overpotential

(A) Parallel manner O_2 adsorption configuration.

(B) End-on manner O_2 adsorption configuration.

(C) The linear relationship between Gibbs free energy of adsorbed oxygenated intermediates including *OO, *O, and *OH on various metal surface.

(D) The heatmap of limiting potential combining the scaling relationship between G_{OOH} and G_{OH}, which also includes the performance of various 2D materials. Reproduced with permission from[39] copyright 2018 American Chemical Society.

The oxygen catalytic reaction cycle process is four electrons reaction steps. Precisely, in alkaline electrolytes, OER starts with the adsorption of OH^-, by generating an *OH free radical. It is followed by the deprotonation of *OH with forming *O accompanied by one electron and one water molecule released. The coupling of adsorbed *O and *OH generates the *OOH intermediate which further conducts with a proton-coupled electron transfer process and produces an oxygen molecule and a free-active site (*). The kinetics of OER is mainly determined by the binding strength of oxygen adsorbates such as *OOH and *O intermediate on the active sites.[24] The formation of *OOH is generally recognized as the rate-limiting step, hence the *OOH adsorption free energy (ΔG_{OOH}) is normally treated as the descriptor of OER overpotential (η^{OER}).

ORR mechanism

ORR is widely employed as the cathode reaction in various next-generation energy conversion cells. Actually, ORR process acts as either dissociative or associative, induced by the different oxygen adsorbed models and dissociated barrier on the surface of electrocatalysts. There are two reaction models of ORR: (1) the direct four-electron pathway based on parallel manner O_2 adsorption configuration (Figure 3A), and (2) the indirect four-electron pathway mediated by the end-on manner O_2 adsorption configuration (Figure 3B). The indirect four-electron pathways are composed of two parts. Firstly, the end-on adsorption O_2 molecule changes to H_2O_2. Secondly, H_2O_2 undergoes another two-electron process to produce H_2O. Generally, the ORR performance following the indirect four-electron reaction path is relatively poor related to that of the direct four-electron pathway.[38]

The direct $4e^-$ pathways of ORR are outlined as follows:

$$* + O_2 + H_2O\ (l) + e^- \rightarrow *OOH + OH^-\ (aq) \qquad \text{(Equation 6)}$$

$$*OOH + e^- \rightarrow *O + OH^-\ (aq) \qquad \text{(Equation 7)}$$

$$*O + H_2O\ (l) + e^- \rightarrow *OH + OH^-\ (aq) \qquad \text{(Equation 8)}$$

$$*OH + e^- \rightarrow * + OH^- (aq) \quad \text{(Equation 9)}$$

The indirect $4e^-$ pathways reaction equation is as follows:

$$O_2 + H_2O (l) + 2e^- \rightarrow HO_2^- + OH^- (aq) \quad \text{(Equation 10)}$$

$$HO_2^- + H_2O (l) + 2e^- \rightarrow 3OH^- (aq) \quad \text{(Equation 11)}$$

Overall in either direct or indirect $4e^-$ pathway, as shown in Equation 12:

$$O_2 (g) + 2H_2O + 4e^- \rightarrow 4OH^- (aq) \quad \text{(Equation 12)}$$

The ORR process involves multi-elementary steps including O_2 adsorption, hydration, peroxide/oxide formation, and desorption of surface hydroxide. At the early work, the adsorption Gibbs free energy of the key intermediates in ORR process were calculated by density functional theory (DFT) in Nørskov's work. It was found the overpotential is generated by the thermodynamic limiting potential (U_L), which can be defined as $\eta = \Delta G_{max}$ (ΔG_{OOH}, $\Delta G_{OH,}$ and ΔG_O)/e. Remarkably, there exists a linear relationship between the binding Gibbs free energies of the three intermediates ($\Delta G_{OOH} = \Delta G_{OH} + 3.2 \pm 0.2$ eV and $\Delta G_O = 2\Delta G_{OH}$) as shown in Figures 3C and 3D, and the U_L is also a function of ΔG_{OOH} and ΔG_{OH}. Thus, the adsorbed Gibbs free energies of the three oxygenated intermediates are identified as the earliest ORR activity descriptor.[39]

For acid solution, the $OH^- - e^-$ in Equations 1, 2, 3, 4, 5, 6, 7, 8, 9, 10, 11, and 12 instead by $H^+ + e^-$, and the Gibbs free energy of $H^+ + e^-$ can be related to $OH^- - e^-$ according to Equations 13 and 14. Thus, in both alkaline and acid solution, the key intermediates are O*, OH*, and OOH*[40] and act as the activity feature parameters. The reversible transfer rate between water and O_2 molecule are highly dependent on the electron/proton transfer rate at each elementary step.

$$H^+ + e^- \rightarrow 1/2H_2 (g) \quad \text{(Equation 13)}$$

$$\mu OH^- - \mu e^- = \mu H_2O (l) - (1/2\ \mu H_2 (g) - eU_{RHE}) \quad \text{(Equation 14)}$$

where μ are the (electro)chemical potentials of the indicated species.

In either OER or ORR, the redox reactions shown in Equations 5 and 12 require substantial overpotentials. Scaling relationships between limiting potential and binding Gibbs free energy of intermediates can be adopted for increasing the predictive efficiency of novel catalysts. But it still has significant drawbacks on electrocatalysts design due to only considering the adsorption energy. Recently, it was expected the electronic and geometric properties of electrocatalysts are sufficient regarding as descriptors for the OER/ORR performance in the terms of high-throughput computing and ML algorithms.[41]

PROGRESS ON DESCRIPTOR-BASED APPROACH FOR OXYGEN REDOX REACTIONS

The electrocatalytic reaction process of OER/ORR occurs at complicated solid-liquid interfaces influenced by the atomic active site and coordination environment and solvent effects. Therefore, it is necessary to review the descriptors identified from the atomic microscale, cluster mesoscale, and bulk macroscale for feature engineering and materials intelligent design in oxygen redox reaction. In this section, the latest progress and limitation of multiscale descriptors were summarized containing geometric properties, electronic properties, and corresponding composite structures in the application of catalyst design for OER and ORR. The accurate cognition of descriptors effectively promotes the prediction of the performance and design of new materials, which is of great significance for the rapid development of materials in the new era.

Descriptor development for atomic-scale catalysts

Atomic scale electrocatalysts include M-N-C (M: metal) and M_1-M_2-N-C structures, which present high-density active catalytic sites. The TMs-N-C (TMs = Fe, Co, Ni, Mn, etc.) show great performance toward heterogeneous catalysis because of the advantages of superior electrical conductivity and high intrinsic

OER/ORR activity originated from TMs active sites and surrounded nitride/carbon atoms. Compared to TMs-N-C systems, the pure nitrogen-doped carbon-based materials is unbenefited for OER process, which suffer from the rapid oxidation and dissociation with the formation of carbon dioxide above 0.207 V under the high potentials (>1.4 V vs. Standard Hydrogen Electrode [SHE]). The doped TMs in NC material increase the graphitization of systems to suppress the corrosion and charge accumulation in the OER process. Therefore, doped TMs in carbon materials are effective to achieve high performance for both ORR and OER. For transition metal–nitrogen–carbon (TM-N-C) atomic-scale materials, the ε_d, charge transfer, unsaturated coordination number, and another composite descriptor can construct a relationship between activity and intrinsic physical and chemical properties.[42,43]

Adsorption energy of intermediate

Overpotential can directly reflect OER/ORR performance for electrocatalyst and is relative to the adsorption free energy of intermediates. However, the rate-limiting steps are different in OER and ORR processes for TM-NC systems, and it imposes difficulty to construct descriptors from one intermediate for both OER and ORR. Recent studies show that ΔG_{OH}, $\Delta G_{O,}$ and ΔG_{OOH}-ΔG_{O} are the three potential descriptors of overpotential in various TM-NC systems. Waterhouse et al. calculated three key intermediates including OH*, OOH*, and O on 60 different 3*d* -transition metal single-atom systems (3*d*-TM-SACs) with symmetric and asymmetric coordination environment. The symmetric configurations (TM-N_x-C) is composed of various nitrogen numbers (x = 4, 3, 2), and the asymmetric configuration (TM-N_3X-C) consists of nitrogen and various non-metal elements (X = P, S, B). The adsorbed Gibbs free energy of OOH* and O* have a linear relationship with ΔG_{OH}, and combining the consistent limiting rate step in most TM-N-C systems, thus the performance can be described by the binding strength of a single intermediates. Differently in rate-limiting step of TM-N_4-C systems (TM = 3*d*, 4*d*, 5*d* metals), the adsorbed Gibbs free energy of O* intermediate was identified to be a key parameter in describing the catalytic activity (Figure 4C).[44] In double metal atom systems (M_1M_2-N-C) that the FeFe, CoCo, NiNi, CoFe, CoNi, and FeNi biatoms as well as their coordinated eight nitrogen atoms are embedded in carbon layer.[45] The structure-property descriptors are different in OER and ORR due to their different rate-limiting step. The adsorption free energy of *OOH intermediate was found to have a linear scaling relationship with ORR overpotential, and the ΔG_{OOH}-ΔG_{O} can be also regarded as a descriptor to construct a volcano plot with OER overpotential (Figures 4D–4G). Based on those descriptors, Co-N-C and Rh-N-C were identified to present optimal performance for both OER and ORR, which are the potential bifunctional electrocatalysts.

d electronic descriptors

The *d*-band center theory was proven to be an efficient and classical indicator for the free energy change of the key intermediates.[46,47] The energy contributed by the *d*-band electrons (ΔE_d) is mainly composed of bonding states (ΔE_d^{ortho}) and antibonding states ($\Delta E_{d\text{-hyb}}$), leading to the Pauli repulsion between adsorbates and 3*d*, 4*d* and 5*d* TMs. Thus, the ΔE_d term can be expressed as follows:

$$\Delta E_d = \Delta E_{d\text{-hyb}} + \Delta E_d^{ortho} \quad \text{(Equation 15)}$$

There also exists *sp*-band in TMs, which originates from the valence *s* and *p* orbitals in a broad overlapping shape. The research exhibited that energy contribution from free electron-like *sp* electrons is independent of the metals, which implies that the adsorption energy for the adsorbates is directly related to the *d*-band electronic states.[47] The ε_d is the simplest descriptor for the *d*-band electrons, in which the positive shift of ε_d toward the Fermi level indicates the stronger interaction, while a negative shift of ε_d is accompanied by weaker interaction.

The TM-NC catalysts are currently the hot spot materials for bifunctional catalysts. Accurately predicting their active site becomes very important but challenging. Neither experiment nor theoretical modeling can traverse all possible single-atom structures quickly with low cost. Recently, on the basis of the cross-validation scheme of DFT and machine learning, the fundamental relationship between geometric/electronic structure and OER/ORR overpotential can be easily obtained by the best-performing machine learning model in the TM-NC systems. It was declared that the ε_d was proved to be the important descriptor in various TM-N-C atomic scale catalysts.[14,48]

Guo and coworkers investigated 3*d*-4*d*-5*d* TM atoms embedded in different coordination C-N numbers consisting of C_3N, C_2N, C_3N_5, C_4N_3, $C_3N_{3,}$ and C_3N_4 (Figure 5A).[48] The calculated Gibbs free energy

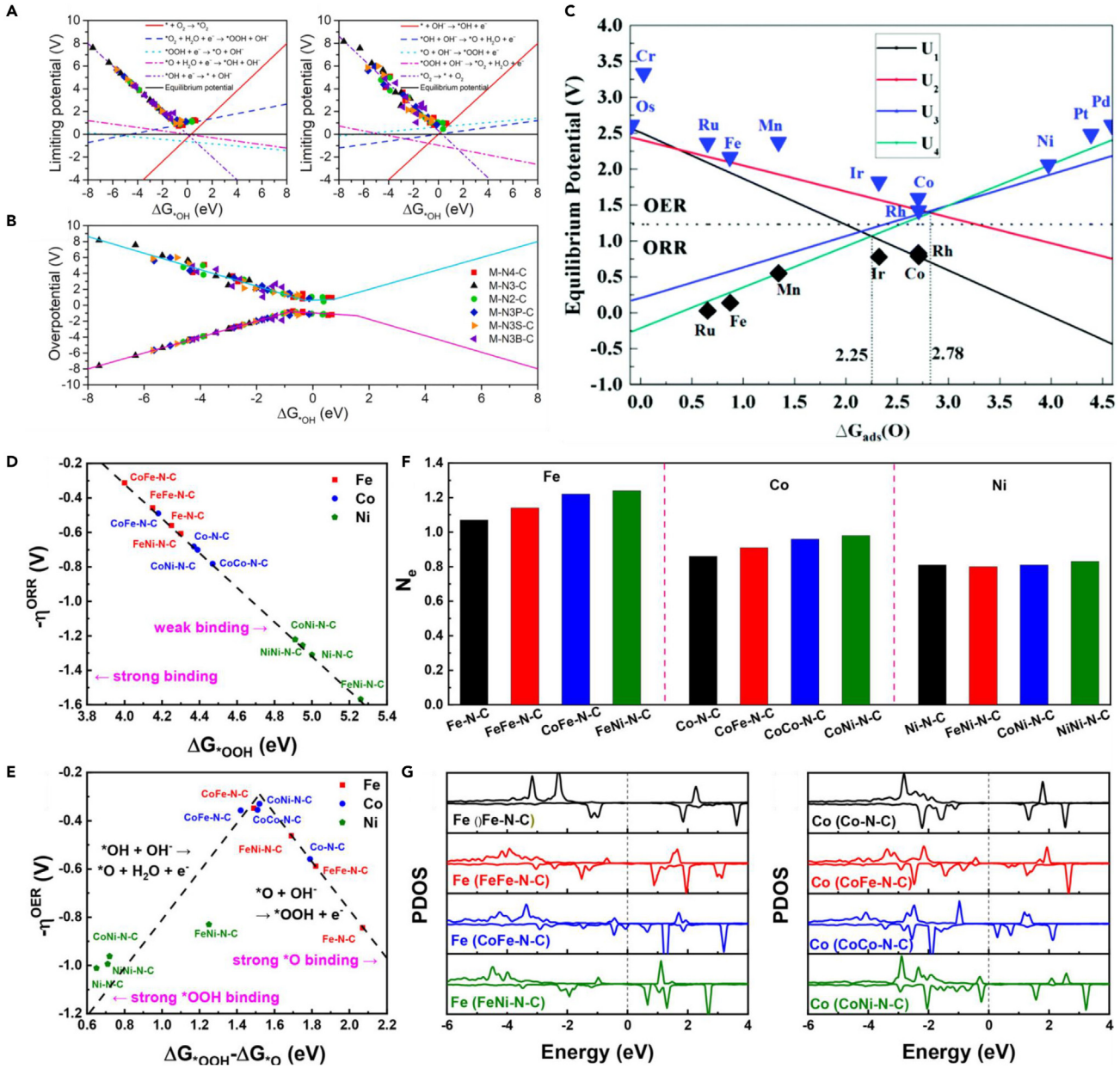

Figure 4. The different intermediate descriptors and corresponding electronic state in the metal-nitride-carbon system

(A) The scaling relationship between OER/ORR limiting potential and ΔG_{OH} in 3*d*-TM-SACs systems.

(B) The dual volcano plot of OER/ORR overpotential for 3*d*-TM-SACs systems. Reproduced with permission from[18] copyright 2022 Elsevier.

(C) Thermodynamic volcano plot between OER/ORR performance and ΔG_O for TMs-N_4-C systems.

(D) ORR theoretical overpotential (η^{ORR}) versus ΔG_{OOH}.

(E) OER theoretical overpotential (η^{OER}) versus ΔG_{OOH}.

(F) The charge transfer number in TMs-N-C (TM = Fe, Co, Ni) systems.

(G) Projected electronic density of state of TMs-N-C (TM = Co, Fe) systems. Reproduced with permission from.[45] Copyright 2018 American Chemical Society.

can be well fitted by various ML models, thus the ML model training result can accurately predict the catalytic activity in the use of TMs-N-C systems. The result shows that RhPc, Co-N-C, and Rh-C_4N_3 are the three promising oxygen electrocatalysts with low overpotential. As shown in Figures 5B and 5C, the importance of various feature parameters was analysis by random forest regression (RFR) models. The electron number of the *d* orbital (e_d) is the most importance features for both OER and ORR with feature importance of 40.62% and 48.94%. Even though the *d* electron is the most important descriptor, the thermodynamic

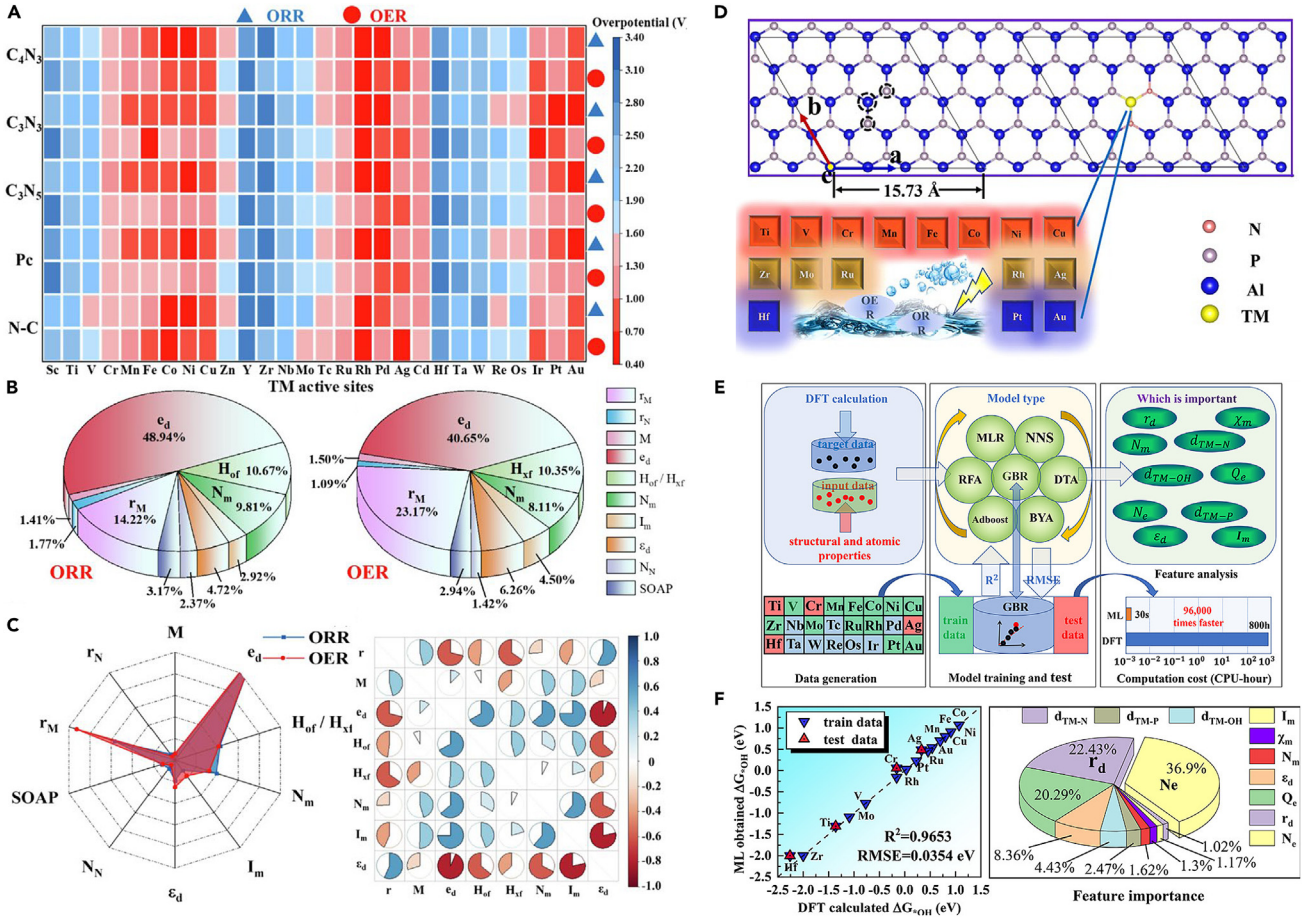

Figure 5. ML fitting and feature importance analysis in different atomic models including TMs-NC and TM@VAl-2Np-AlP

(A) Heatmap of ML-predict limiting potentials in OER and ORR of TMs-N-C systems.

(B) The feature importance analysis by RFR models of various feature parameters for OER and ORR.

(C) The radar comparison chart on the RFR analysis feature importance of various feature parameters on the feature importance of features in the RFR models for OER and ORR. Reproduced with permission from[48] copyright 2018 Elsevier.

(D) Atomic models of TM@VAl-2Np-AlP-based substrate and corresponding TM elements as SAC candidates.

(E) Brief description of the ML process.

(F) The scaling relationship between DFT calculated and ML fitted ΔG_{OH^*} value and corresponding feature importance analysis by ML models. Reproduced with permission from[49] copyright 2022 American Chemical Society.

and geometric properties such as enthalpy, coordination number, and atomic radius are still factors to be reckoned with. By combining DFT and ML method, that work opens a new approach for rational and low-cost design principle of ideal catalysts by exploring the importance ratio of different features to predict and design a new class of OER/ORR electrocatalysts.

The two-dimensional nanomaterials present novel physical and chemical properties, including robust mechanical properties, high specific surface area, and abundant active sites. The *d*-band center descriptor is also suitable as descriptor for the two-dimensional TM-semiconductor substrate such as transition-metal sulfide, phosphide, and nitride. Deng's group investigated the OER performance of the graphene-like GaN monolayer doped with TM atoms (3*d* metals, Ru, Pd, Pt, and Au). The results showed that M/g-GaN (M = Fe, Ni, Au) can be used as a highly active bifunctional catalyst. ΔG_{OH} and ΔG_{OOH} are linear related to the TM atomic *d*-band centers.[50] Zhang and coworkers explored the AlP monolayer based on the TM and nitrogen doping through theoretical modeling.[49] They achieved higher OER/ORR activity by replacing two P atoms with two nitrogen atoms in the TM-anchored AlP monolayers (Figure 5D). Furthermore, the ε_d, *d*-orbital electron number and the electronegativity of the TM atom were identified to be good descriptors of OER/ORR activity in TM-anchored AlP materials. As shown in Figure 5E, after

performing an ML algorithm (GBR, gradient boosted regression), the TM *d*-electron number and charge transfer of TM atoms are the main descriptors of the adsorption behavior, realizing the descriptors from catalyst overall characteristics of atoms. The optimal single-atom catalysts derived by ML can be further verified by DFT calculations to determine the reliability and accuracy of the model (Figure 5F).

Geometry-related descriptors

The geometry-related descriptors have more significant contribution to the atomic-scale electrocatalysts compared to bulk materials, generally including coordination number, bond length, bond angle, space group, and symmetry. In Liu's work, different kinds of Fe-atom doped carbon-defective models were constructed to investigate the relation between performance and the related descriptor (Figures 6A and 6B). The Fe-O bond length at the Fe active site and adsorbed O_2 molecule is the descriptor that accurately predicts the ORR overpotential in Fe-N_4-C with various defective systems (Figure 6C).[19] Li's group proposed a data-driven high-throughput design principle by combining DFT and ML. In this work, the intrinsic descriptor (Equation 16) contained geometric and electronic structure in all 3*d*, 4*d*, and 5*d* biatoms doped defect nitrogen-doped carbon structure was constructed (Figure 6D). The theoretical results achieved by the data-driven high-throughput design principle shows that there exist 511 and 855 types of double-atom catalysts (DACs) superior than IrO_2 and Pt in OER and ORR activity. They also found 248 kinds of bifunctional DACs presenting superior catalytic activity for both OER and ORR (Figures 6E and 6F). The intrinsic descriptor (Equation 16) is as follows:[51]

$$\varphi = \frac{\overline{\theta}_d^2 \overline{\chi}}{N_C \chi_C + N_N \chi_N} \quad \text{(Equation 16)}$$

θ_d is the valence electrons of metal elements, χ is the electronegativity and *N* and C are the number of nitrogen and carbon atom coordinated with the metal, respectively.

Composite descriptors

The application of ML endows more convenient and accurate descriptors in OER/ORR. Compared to the one-component descriptor, the multi-component descriptor including the *d*-band center theory, coordination environment, electronegativity, and ionization energy is more accurate to predict OER/ORR activity. The key process is extracting important feature parameters from hundreds of physical and chemical parameters. ML algorithm becomes very effective to filter the different feature parameters and construct the multi-component descriptor.[12] Huang et al. performed ML model training based on the RFR to find the performance descriptors for OER/ORR. Precisely, the number of electrons and the enthalpy change for oxide formation were found to be two important factors to affect the bifunctional OER/ORR activity of single-atom catalysts. Moreover, the data-driven high-throughput design principle was proposed to estimate the stability and activity of diatomic structures in OER. The effective approach with a high prediction accuracy of $R^2 > 0.926$ lowers the screening time by 1,44,000 times compared to the DFT method. This data-oriented research method greatly accelerates the design and discovery of high-performance diatomic catalysts.

Xia and coworker constructed a series of structures of X-doped carbon (X = N, B, P, S, Si, Se, Sb, F, Cl, Br, I, POH, SOH, PO_2, SeO_2, SO_2, etc.) (Figure 7A), where Φ, a dimensionless factor defined as shown in Equation 17, can be treated as the bifunctional descriptor to predict the effect of structural characteristics.[52]

$$\Phi = (E_X / E_C) \times (A_X / A_C) \quad \text{(Equation 17)}$$

E_X is the electronegativity and A_X is the electron affinity. By considering the combined effects of the electron adhesion and E_X of the dopant on the redistribution of charge on the systems, the *p*-orbital element doping effect was formulated to predict OER/ORR performance. The finding can be attributed as follows: the ability to form covalent bonds with carbon and the ability to transfer electrons in the reaction, which reduces the overpotential and stabilizes the adsorbate, thereby enabling fast OER/ORR kinetics. Based on the scaling relationship between the binding strength and ORR/OER limiting potential, nitrogen and phosphorus were proved as the optimal doped elements for graphene in applications of OER and ORR, respectively. More precisely, when the composite descriptor (Φ) fluctuates in 1–3 for ORR, 0.5–2 for OER, the predicted performance is superior than the benchmark catalysts of Pt and RuO_2 in ORR and OER. The research shows that the *p*-orbital element-doped graphene have potential to be the bifunctional catalysts for OER and ORR (Figures 7B and 7C).

Additionally, Chen et al. reported alkenyl single-atom configurations (M@C_3, M@C_4, M@pyridine-M_4, and M@pyrrole-N_4).[14] The ML models were used to describe readily available physical properties and fundamental

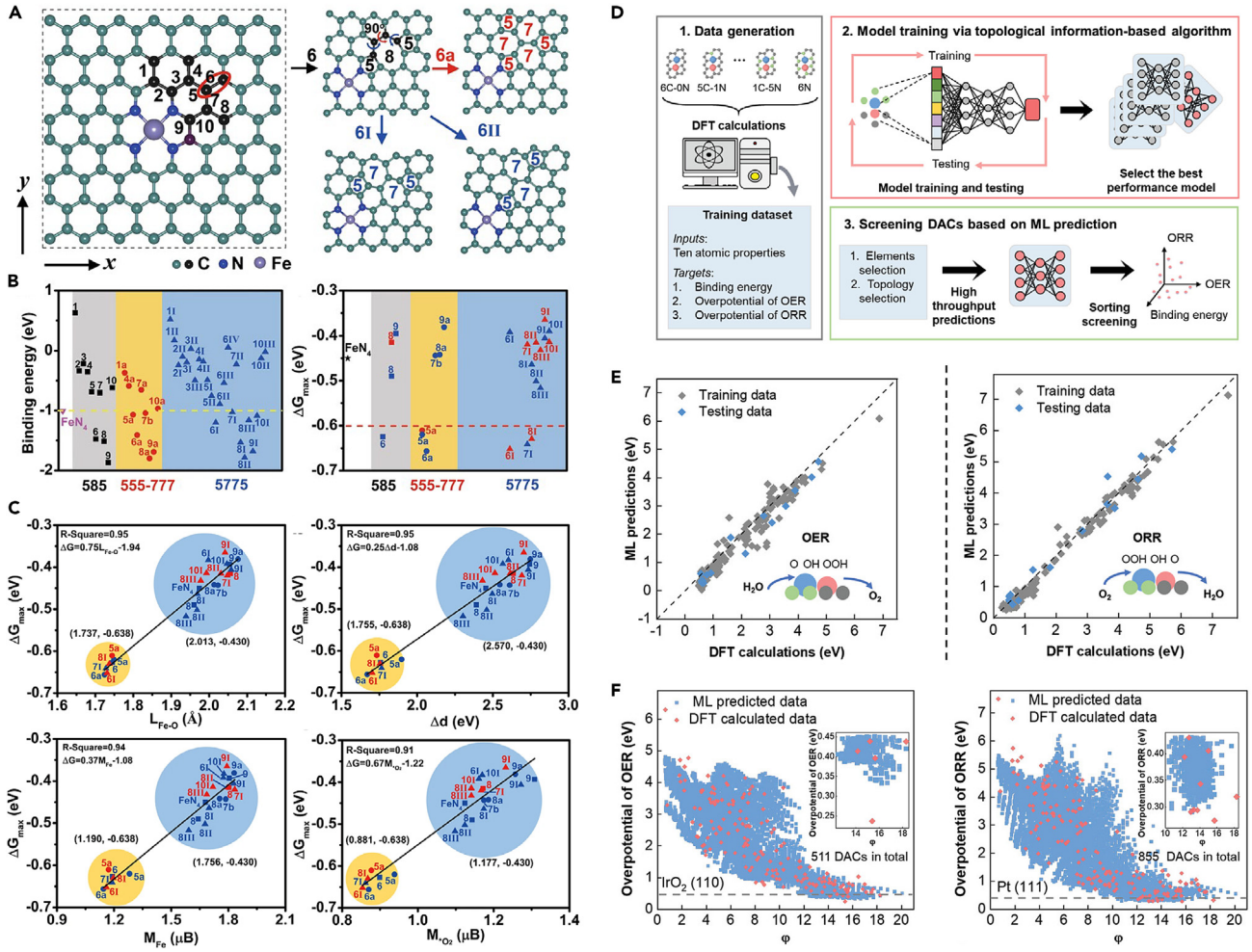

Figure 6. The descriptor of geometric and electronic structure of metal-nitride-carbon models

(A) Optimized structure of perfect and divacancy defect FeN_4 site.

(B) The binding energy of ORR activity of Fe-N_4 site.

(C) The scaling relationship between parameters and limiting potential. The feature parameters including Fe-O bond length, *d*-band center gap of Fe spin state, the spin magnetic moment of Fe and adsorbed *O.

(D) Illustration of the workflow of the topological information-based ML model to screen DACs with an optimal electrocatalytic performance from a vast design space.

(E) The linear relationship between DFT calculated overpotential and ML model fitted and predicted results for OER and ORR.

(F) The overpotential of OER/ORR achieved by DFT calculated and ML model predicted as a function of multi-component descriptors (φ). Reproduced with permission from.[51] Copyright 2022 Wiley-VCH.

modes of limiting potential, predicting 260 kinds of graphene-supported catalysts containing metal N_xC_y active sites. It was found that the top few characteristic parameters in ORR/OER activity are the *d*-band center, oxygen formation enthalpy, electronegativity, H_{xf} (hydride formation enthalpy) and average electronegativity. The accuracy of the ML models in this work were also verified by DFT calculations. Important lines of various descriptors were proposed, which are instructive for the screening and design of structures for similar systems.

Huang's research group regulated biatom embedded g-C_3N_4 structure and built a model containing 26 homonuclear and 253 heteronuclear biatom/C_3N_4 (M_2/g-C_3N_4 and M_1M_2/g-C_3N_4) (Figure 7D).[53] Through the ML technology model training, it is found that the features of *L*, *d*, and $R_{cov\text{-}ul}$ show an obvious effect on catalytic activity (Figures 7E and 7F). Three features are identified as the distance of two metal atoms (*L*), the average bond length between the surrounding nitrogen atoms and metal atoms ($d = (d_1 + d_2 + d_3 + d_4 + d_5 + d_6)/6$), the covalent radius ($R_{cov\text{-}ul}$)). Followed this principle, they identified that AuRh/g-CN with a small overpotential of 0.35 V for ORR and AgPd/g-CN with a small overpotential of 0.43 and 0.48 V for OER and ORR, which can be

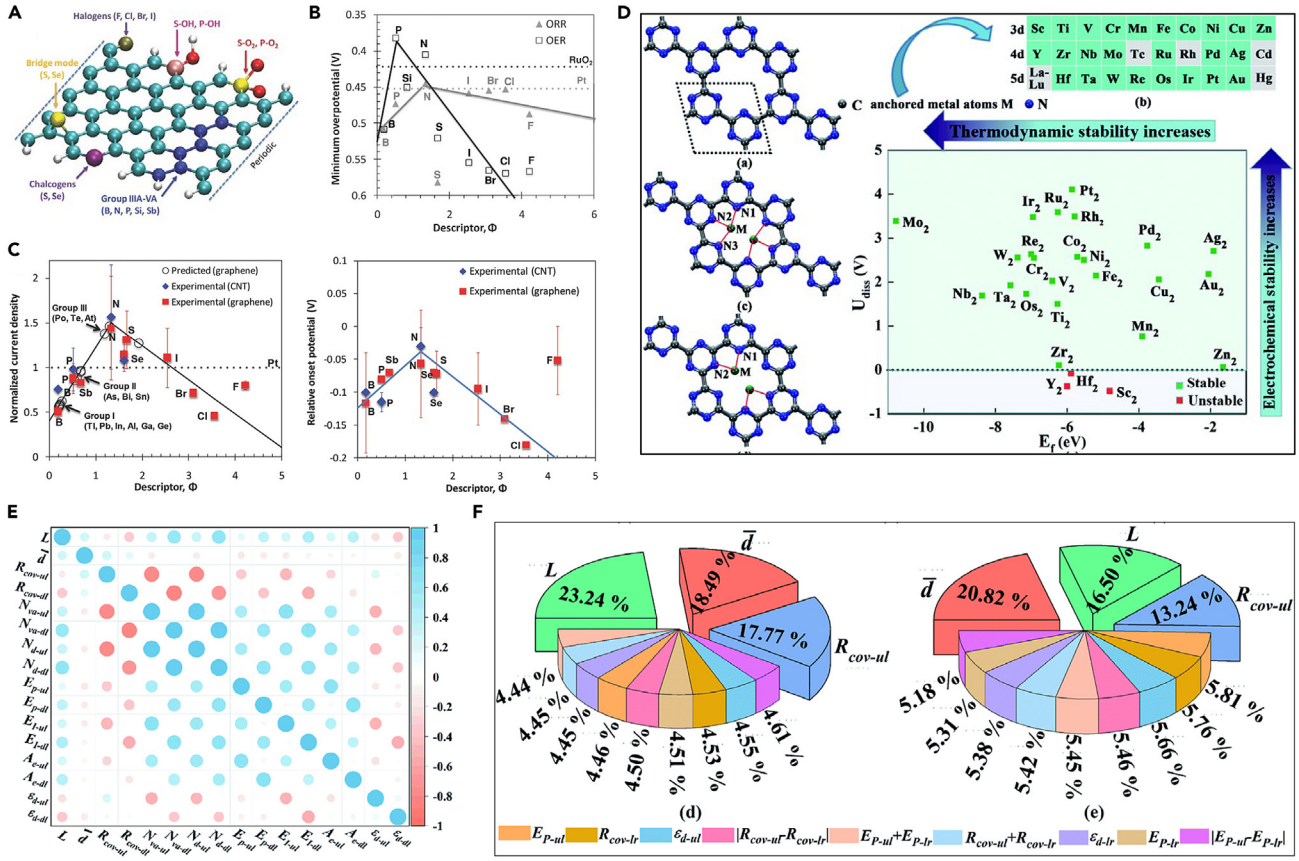

Figure 7. The composite descriptor contained electronic structure and coordination environment controlled OER/ORR performance

(A) Atomic models of the X-doped graphene nanoribbons and corresponding elemental dopant position.

(B) The relationship between OER/ORR overpotential and composite descriptor (Φ).

(C) The limiting current density and onset potential as a function of composite descriptor (Φ). Reproduced with permission from[52] copyright 2022 The Royal Society of Chemistry.

(D) The optimized structure, calculated E_f (formation energy) and U_{diss} (dissolution potential) for M_2/g-CN, considered metal atoms M.

(E) The fitted Pearson correlation coefficient between various selected features of biatom catalysts systems.

(F) The feature importance analysis for OER and ORR overpotential achieved by RFR models fitting. Reproduced with permission from[53] copyright 2022 The Royal Society of Chemistry.

used as a promising bifunctional electrocatalyst. According to the ML analysis and fitting, the other feature parameters such as valence electrons and unpaired electrons in the occupied *d* orbital, Pauling electronegativity, the number of carbon and nitrogen atoms closest to the metallic center were also considered as the contributed descriptor to predict the OER/ORR performance in 3*d*-5*d* TMs-N-C systems.[17] The research shows that the coordinated N/C number is the most importance feature parameters to affect the activity and stability. Among various -N_nC_m moieties, the -N_2C_2 moieties tend to be easily formed and show higher electrochemical catalytic performance and longer durability than other materials such as Pt/Ni- N_2C_2.

Descriptor development for cluster-mesoscale catalysts

Clusters, as the mesoscale materials, are important units that connect the atomic microscale and the bulk macroscale, where their properties differ from single atoms and their bulk material counterparts. Bulk metals have electron band structures, while clusters have discrete electron energies, specific sizes, shapes, and unique electronic structures. The cluster material is usually deposited on the substrate which acts as a composite catalyst. The shape and electronic structure of clusters are also correlated with the substrate properties, and their performance is highly decided by the ensembled properties of the cluster and the corresponding substrate. The unsaturated coordination environment of cluster catalysts and dynamic structure evolution show significant impact on the reaction performance. Extraction of environmental descriptors, therefore, plays a certain role in promoting the intelligent design of cluster catalysts.

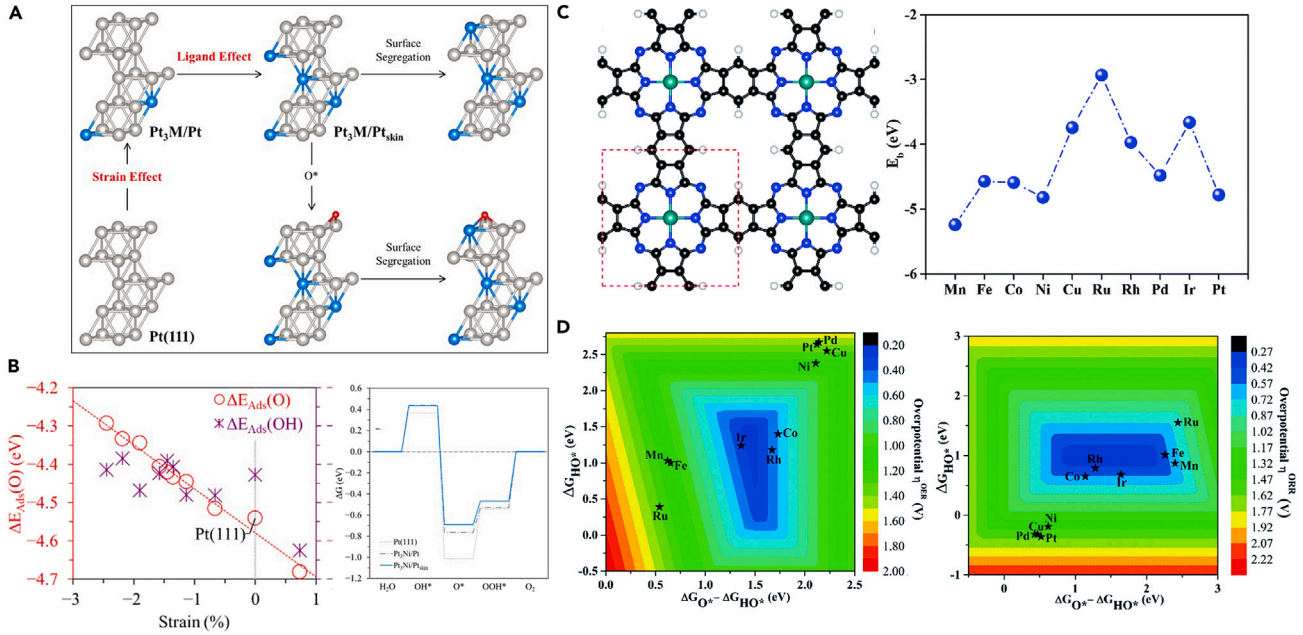

Figure 8. The coordination environment impact of OER/ORR activity for Pt cluster and TM@Pcs materials

(A) The atomic models of Pt_3M/Pt and corresponding adsorbed models.

(B) The strain effect of adsorption energy of *O and Gibbs free energy change of oxygenate intermediates in OER/ORR process. Reproduced with permission from[27] copyright 2021 MDPI.

(C) Optimized geometric configurations and binding energies for the TM-doped phthalocyanine monolayer models.

(D) The colored contour plots show that there exist scaling relationship between the overpotential of OER/ORR and the adsorbed Gibbs free energy of the key intermediate. Reproduced with permission from[55] copyright 2020 The Royal Society of Chemistry.

Coordination environment descriptor

The descriptor for a cluster can be classified into coordination environment, *d*-band electrons distribution, and other composite functions. In Ham's work, the Pt_3M/Pt nanoalloy catalysts (M = 3*d* TM) for OER and ORR were investigated using DFT calculation (Figures 8A and 8B).[27] The strain and ligand effects were found to be the key factors for OER/ORR catalytic activities. Compared to pure Pt crystals with (111) lattice plane exposed, the OER/ORR activities in a Pt_3Ni/Pt_{skin} were increased by 13.7% and 18.4% attributed to the lattice train and ligand impacts. Zhao's work also exhibited that OER/ORR performance depends on the cluster size and metal atomic numbers. Several palladium (Pd*n*, n = 1–6, and 13) nanoclusters anchored on the surface of defective MoS_2 monolayer with S monovacancy were studied. The OER/ORR performance was strongly dependent on the size of the anchored Pd clusters: Pd_6/MoS_2 presents the highest activity toward ORR with a 0.59 V overpotential, and Pd_2/MoS_2 shows the highest activity on OER with a low overpotential of 0.32 V.[21] Juan et al. investigated the impact of structural stability of small Pt clusters with different conformations on Au (111) by employing DFT methods. A triatomic cluster of Pt was found to be more stable on Au (111) with a linear conformation. For clusters with four or more atoms, Pt on Au (111) prefers nonlinear conformation.[54]

Adsorbates descriptor

The adsorbed free energy of the intermediate is also a suitable descriptor of the cluster to describe OER and ORR activity. Wang's research group explored the OER/ORR activity of a single TM atom doped phthalocyanine (TM@Pcs, TM = Mn, Fe, Co, etc.) through a computational screening approach (Figure 8C).[55] In metal-phthalocyanine, there exists a metal-N-C structure in metal-phthalocyanine, which was verified as the active site for ORR. Based on the different rate-limiting step in OER and ORR, the ΔG_{OH} and ΔG_O - ΔG_{OH} were considered as the independent descriptors for OER and ORR, respectively. Rh@Pc were considered as the potential bifunctional electrocatalysts due to low overpotential of 0.44 V in OER and 0.55 V in ORR (Figure 8D). Meanwhile, the metal center can be tightly bound with phthalocyanine monolayers confirmed by the high diffusion energy barriers, leading to the anti-aggregation of metal centers.

The surface active site of the cluster and the coverage of adsorbates both contribute to the OER/ORR performance. The adsorption surface is not a clean surface during the catalytic process but a dynamic surface including various adsorbed intermediates and solvents. Pei's research showed that the alkaline conditions with the pre-adsorption of hydroxyl groups are beneficial for the OER and ORR in hydroxyl group modified single metal and bimetal atoms supported on defective graphene (denoted as HO-M/DG and $(HO)_2$-M^1M^2/DG, M = Ni, Co, Fe and M^1, M^2 = Ni, Co, Fe). While the pre-adsorption of hydroxyl groups is not profitable for HO-Ni/DG hybrid, due to the unstable adsorbed of *OH, *O, and *OOH in OER and ORR process.[56] Hence, the HO-Ni/defective graphene cannot be recognized as an effective oxygen redox electrocatalyst. Understanding the catalytic mechanism of the surface cluster configuration and dynamic change in the OER/ORR process would be a challenge (Figures 9A–9C).

Composite descriptor

The cluster-scale structure has abundant unsaturated coordination active sites and has a good fine-tuning effect on its edge performance with the change of size. It was found that the smaller the size of amorphous carbon is, the more edges the system will have, which exposes with rich active sites. The exposed edge sites facilitate the performance of oxygen redox electrocatalysis. While in Sun's group, they found that the basal carbon in small carbon cluster were considered as the optimal active sites. They doped oxygen groups in the amorphous carbon cluster according to the CO_2-assisted ball-milling process. On the basis of quantum chemical calculations, the *OOH is the key intermediates as a function of overpotential and controlled by the composite electronic descriptor of radical Fukui function. The Fukui function can describe the adsorption capability of the rate-determined intermediate *OOH and it indicates that the carbon atom located at the center of the total carbon cluster is considered as the most active site in H_2O_2 production, defined as follows (Equation 18):

$$F_k^0 = \frac{1}{2}\left[p_k(N+1) - p_k(N-1)\right] \quad \text{(Equation 18)}$$

The $p_k(N + 1)$ and $p_k(N - 1)$ are the electronic populations of atom k in the cases when the carbon surface obtains and loses one electron, respectively.[22]

Descriptor development for bulk macroscale catalysts

The bulk macroscale catalysts, such as TM oxides/sulfides, metal alloys, and molecular organic frameworks have emerged as one of the most promising catalysts for oxygen redox catalysis. Among the kinds of bulk catalysts, TM oxides are the traditional bifunctional catalysts, owing to the unique surface oxygen coordination structure, the advantages of corrosion resistance in alkaline media, moderate cost, and low environmental hazards.[57–59] A plentiful of common TM-based catalysts including binary oxides M_xO_y (M = Mn, Co, Ni), bimetallic hydroxyl oxides (M'M''OOH, particularly with M', M' = Fe, Ni), spinel, conventional perovskites AMO_3, and quadruple perovskites (AMn_7O_{12}, A = Ca and La) were progressively investigated in recent years. The macroscale TM oxides display the unique characteristics of diverse active sites, atomic coordination structures, and adsorption models of intermediates (bridge-cis and top-ads). Their intermediate descriptors (ΔG_O-ΔG_{OH} for OER and ΔG_{OH} for ORR) and the multi-component descriptors including physical and chemical properties are complicated in the electrocatalytic process. Decades of research show that the electronic spin structure of the active metal center is the main factor that affects the OER and ORR activity, directly correlating to the adsorption free energy of intermediates. Those electronic structures of materials are mainly inherited from the coordination environment of bulk TM oxide, and thus, the bulk descriptors comprise electron filling in the *d*-shell and e_g* orbitals, *d*-band center, oxygen *p*-band center, and charge transfer energy.[60,61]

d electronic descriptors

The electron-filling state of *d* orbitals is always a useful descriptor to describe the relationship between adsorbed intermediate and OER/ORR electrocatalytic activity.[29,62,63] The model proposed by Zaanen, Sawatzky, and Allen (ZSA model) is an early theory that has great potential in describing OER/ORR activity and predicting semiconductor band structure in the early stage. It was observed that the potential energy induced by the interaction is not the most critical factor of the energy band but is the magnitude of the charge transfer energy (Δ) which is defined as the energy of an electron transferring from *p* orbital in ligand to *d* orbital in TM. Kirsanova's group investigated the activity of $YBaCoO_{7+\delta}$ structure by using ZSA models.[64] The OER rate-limiting step is linearly related to Δ (charge transfer energy of O 2*p* band separated from upper Hubbard bands), while the ORR rate-limiting step is related to *U* (the energy difference

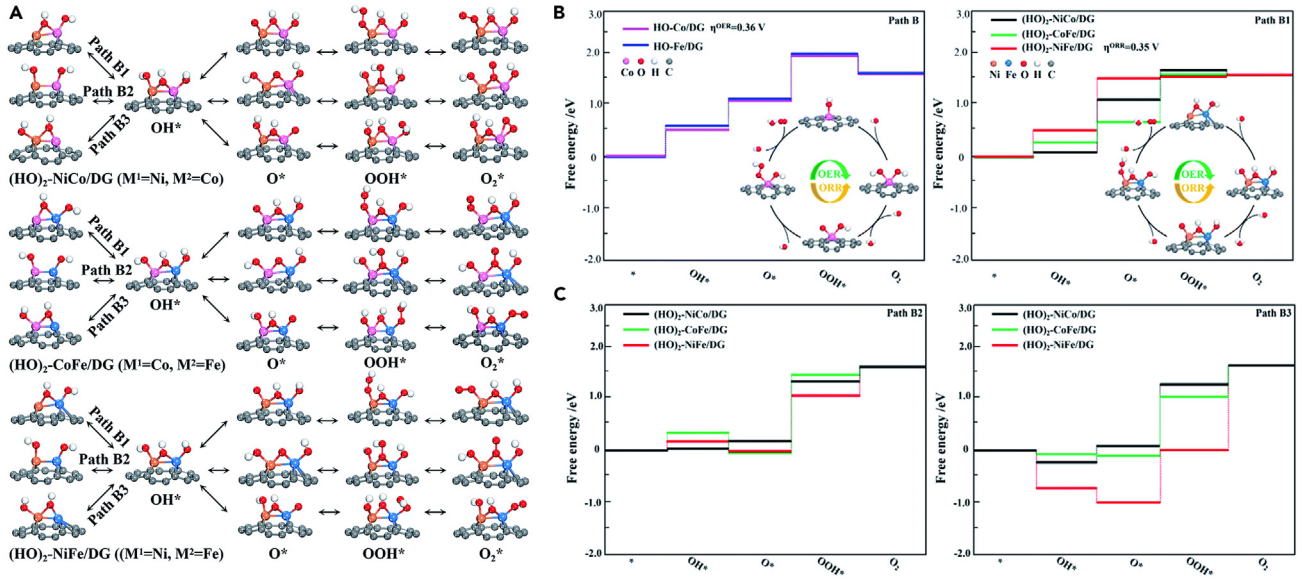

Figure 9. Different OER/ORR paths influenced by adsorbate *OH species for HO/$(HO)_2$-MM/DG

(A) The adsorbed atomic models of $(HO)_2$-MM/DG with adsorbed intermediates including *OH, *O, *OOH and O_2*. The three paths exhibit the different initial adsorption mode.

(B) The free energy diagrams of oxygen redox processes on the surface of various HO-M/DG and $(HO)_2$- M^1M^2/DG models follow Path B1.

(C) The free energy diagrams of oxygen redox processes on the surface of various HO-M/DG and $(HO)_2$- M^1M^2/DG models follow Path B2 and Path B3. Reproduced with permission from[56] copyright 2019 The Royal Society of Chemistry.

of *d*-manifold split band of upper and lower Hubbard band, induced by *d*-orbital Coulomb repulsion). It indicates that the Coulomb repulsion is a key factor for the rate-limiting step of ORR and OER. It was also found that the metal active site in the tetrahedral structure has a larger *U* value and higher ORR activity, endowing the tetrahedral-coordinated Co the catalytically active center (Figures 10A and 10B). Andersen's group verified that the existing *d*-bandwidth is the effective descriptor of *O adsorption enthalpy change through the compressive sensing method. They added the coordination atoms with the adsorbate, ionization potential and the Milliken electronegativity in the descriptor.[65]

The *d-band* theory is also expanded to investigate dynamic processes in the oxygen redox reaction. In Kang's work,[15] the dynamic surface engineering occurring on perovskite $LaMnO_3$ structure in OER/ORR process and was studied to determine the *in-situ* catalytic mechanism of oxide catalysts. They found that OER/ORR performance is highly correlated with the e_g band of the surface metal atoms and charge transfer between adsorbates and surface oxygen atoms. The surface *d* electronic state directly impact the binding strength of the key oxygenated intermediates. Kim and coworkers proposed that the reduced gap between *d*- and *p*-band centers ($\Delta E_{d\text{-}p}$) of $Sm_{0.5}Sr_{0.5}CoO_{3-\delta}$ can improve the OER/ORR activity, showing that the overpotential is controlled by either δ or oxidation states of TMs (Figure 10C).[66]

Apart from TM oxide, MXene is a general term for a class of two-dimensional metal carbides, nitrides or carbonitrides with the chemical formula $M_{n+1}X_nT_x$ (T stands for surface O and F functional groups), due to its excellent electrical conductivity, chemical stability and tunable chemical surface. The local electronic environment and coordination environment of MXene can be effectively regulated by a surface atomic modification to optimize catalytic performance. In Zhang's theoretical work, they explore the OER/ORR performance of atomically dispersed binary Fe/Co/Ni sites embedded in Ti_2CO_2. The thermodynamic and kinetic stability of nine diatomic models were used for OER/ORR bifunctional catalysts. The *d* electrons and work function were explored as useful descriptors to investigate the bifunctional catalytic performance and electronic structure of FeCoNi diatomic/Ti_2CO_2 catalysts.[67]

e_g orbital filling descriptor

The e_g orbital filling is another normal descriptor for TM oxide system, predicting electron spin state, outer electrons, and occupancy that is directly related to the adsorption enthalpy of O-containing

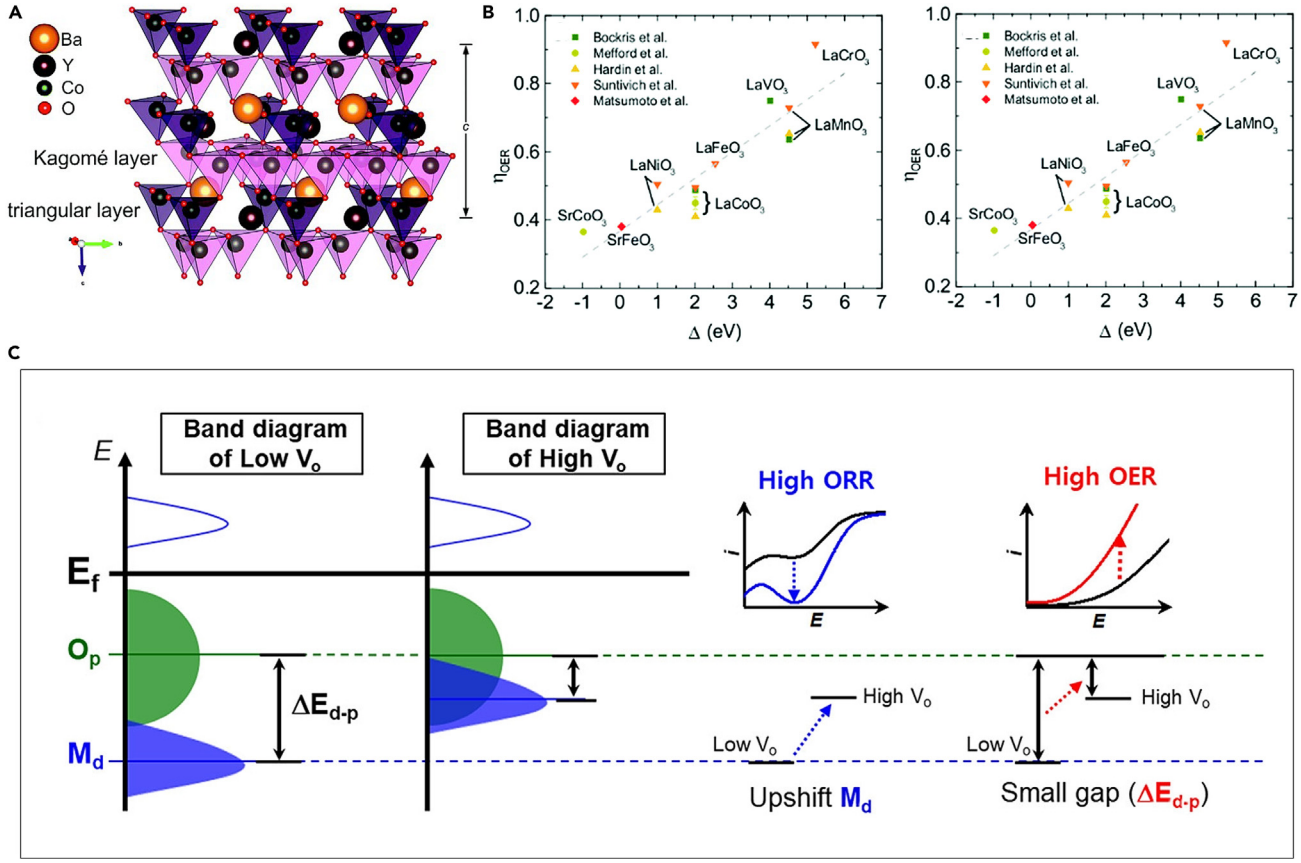

Figure 10. The atomic models and OER/ORR performance controlled by *d* orbital electrons of $YBaCo_4O_7$ systems

(A) Atomic structure of $YBaCo_4O_7$ crystal.

(B) The scaling relationship between OER/ORR overpotential and electronic features including Coulomb on-site repulsion energy (*U*) and charge transfer energy (*Δ*) for perovskite oxide systems. Reproduced with permission from.[64] Copyright 2019 The Royal Society of Chemistry.

(C) The change of band diagrams for different TMOs. Reproduced with permission from.[66] Copyright 2020 American Chemical Society.

intermediates.[16] Xu's research group (Figures 11A and 11B) investigated the OER/ORR performance descriptors of a series of $MnCo_2O_4$ structures.[35] They found that the activity of Mn depends on a volcano-type curve of e_g occupancy, indicating that the activity of the octahedral-based Mn element is manipulated by the filling state of the e_g orbital. Qiu's research group calculated the e_g electron change of Co sites in high-entropy oxide structures through the DFT method (Figures 11C and 11D).[23] AlCoFeMoCr composition shows the highest OER performance among different kinds of high-entropy oxides, in which e_g is closest to 0. Additionally, the e_g orbital filling also depends on the dimensional and size of TM oxide. Chen et al. prepared three-dimensional nanospheres and one-dimensional nanowires $LaNi_{0.3}Mn_{0.7}O_3$ materials and found that the Mn^{3+} ions in the one-dimensional nanowire structure presents a higher spin degree of *t3* 2ge1g, thereby leading to the better catalytic performance with regarding to the low spin degree three-dimensional nanospheres counterpart (Figure 11E).[68] For ABO_3-type catalysts (*A* = La, $La_{0.5}Sr_{0.5}$, Sr, *B* = Mn, Fe, Co, Ni), OER and ORR behavior can also be well-described by unpaired valence electrons (*N*) and nominal valence charge (*V*) of *B* atom in the bulk ABO_3.[37] While the relationships between the electronic state and the catalytic activity for OER and ORR show different trends in many Ni-based and Mn-based systems. The difference mainly originated from the various dynamics in OER and ORR process. There exist linear correlation and second-order reaction relationship between Ni/Mn 3*d* density of states and OER/ORR performance, respectively.[69]

Geometry descriptors

Ham's group performed DFT calculations to study and predict the properties of Pt-based Pt_3M/Pt nanomaterials, aiming to design superior bifunctional alloy OER/ORR electrocatalysts.[27] The stability of

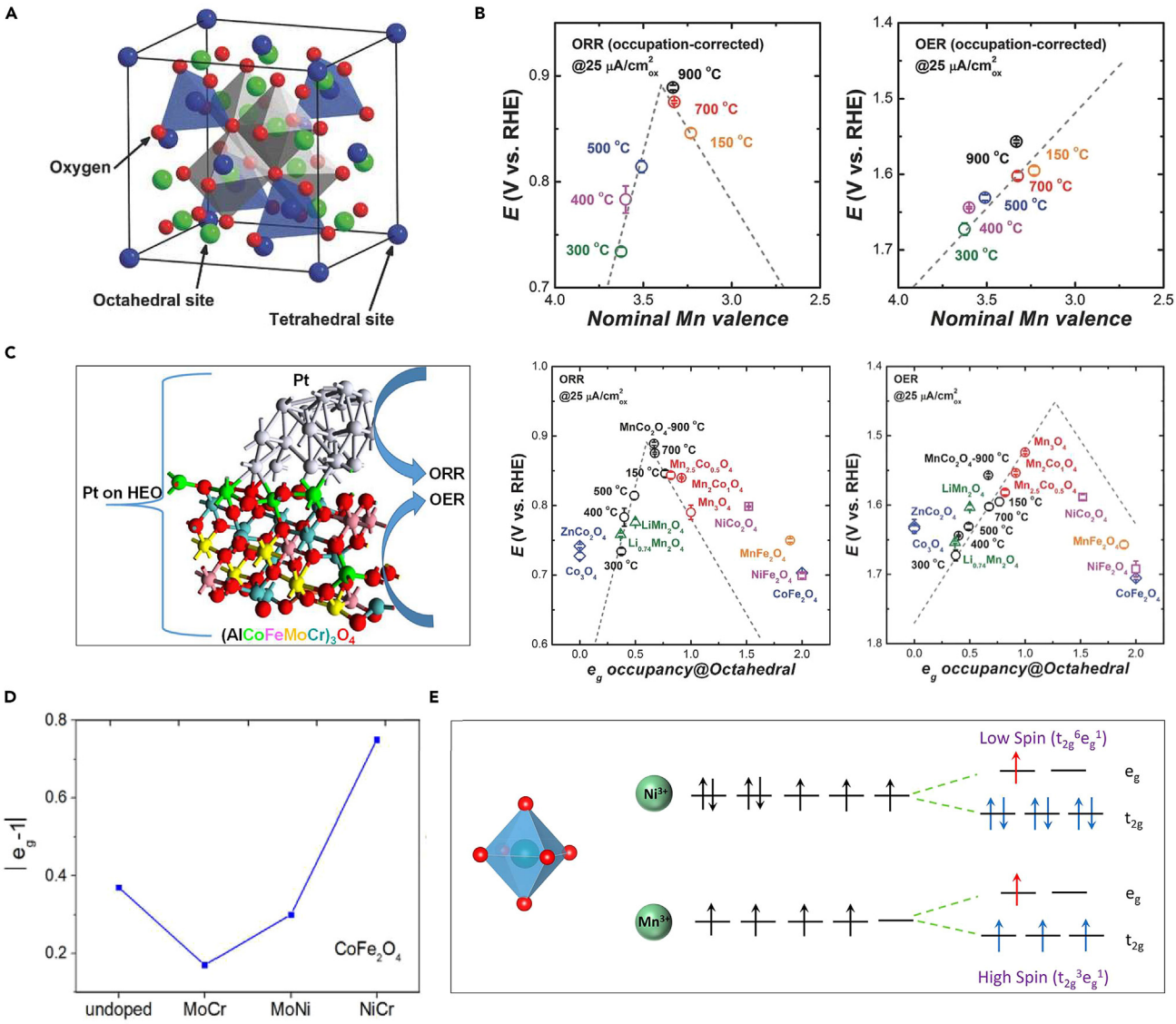

Figure 11. The relationship between e_g orbital filling and OER/ORR performance

(A) Spinel crystal structure with the octahedral site and tetrahedral site.

(B) ORR/OER limiting potential as a function of nominal Mn valence state on various $MnCo_2O_4$ spinels. Reproduced with permission from.[35] Copyright 2017 Wiley-VCH.

(C) Atomic structure of the doped $CoFe_2O_4$.

(D) $|e_g\text{-}1|$ of the surface Co in doped and undoped spinel $CoFe_2O_4$. Reproduced with permission from[23] copyright 2021 American Chemical Society.

(E) Schematic illustration of the BO_6 octahedra structure and electron configurations of t_{2g} and e_g orbitals of Ni^{3+} and Mn^{3+} in $LaNi_xMn_{1-x}O_3$. Reproduced with permission from.[68] Copyright 2022 American Chemical Society.

Pt_3M/Pt catalysts was calibrated by volume formation energy against surface separation energy. The thermodynamic rate-limiting steps were discussed by calculating the adsorption energy of intermediates in the OER/ORR reaction. The catalytic activity and stability are highly relevant to a series of geometric properties including the strain, core structure, lattice distance, and coordination environment, change of the core lattice distance and surface atomic coordination. Xia's work explored the performance of the core-shell structure of $Ag_{32}X_6$ and found that the shell stress of the core-shell structure can be used as an effective descriptor to describe the activity of bifunctional catalysts.[70] In $Ag_{32}X_6$ core-shell structures, the compressive stress induces a more positive charge on the surface of the shell, leading to a higher catalytic activity. Zhang's group constructed a series of biatom doped Ti_2CO_2 structures and

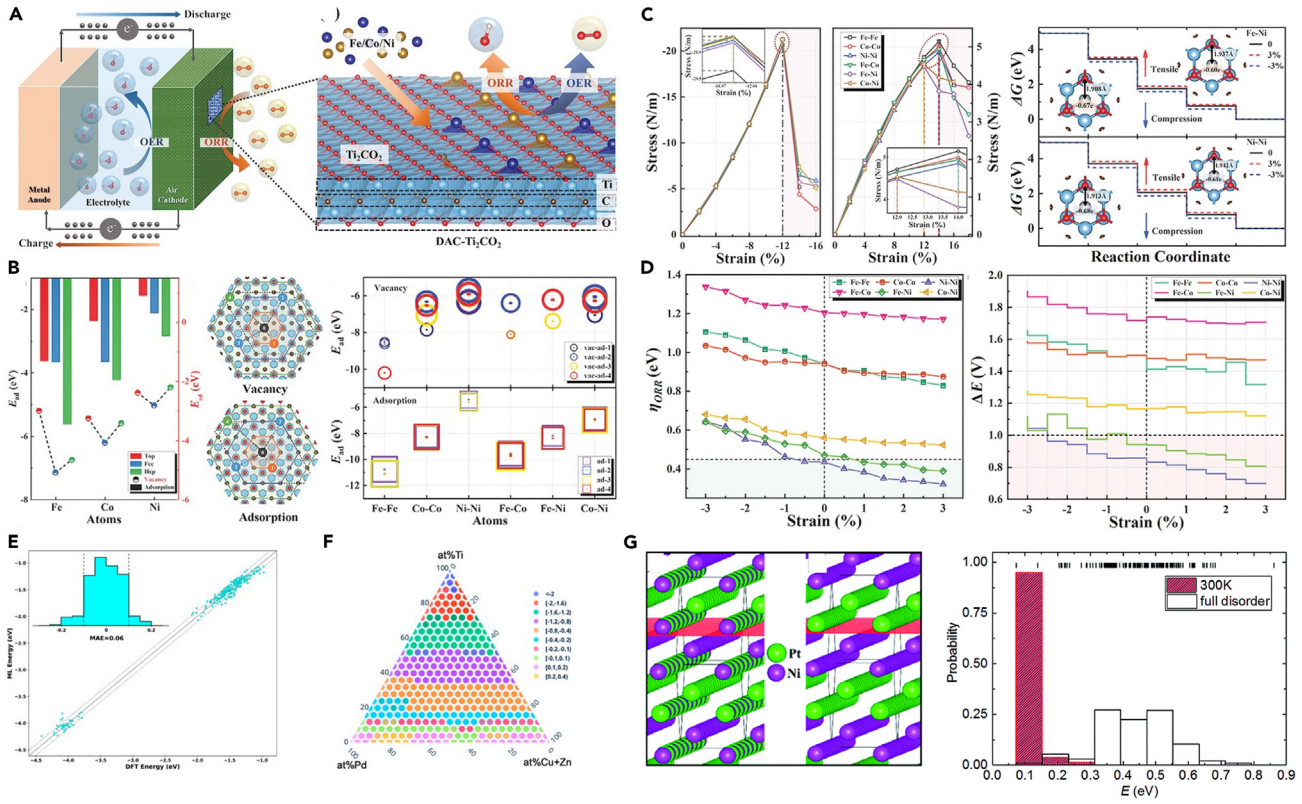

Figure 12. The geometry descriptor of related performance and atomic structure models

(A) The schematic diagram of secondary metal-air battery and corresponding electrode atomic models of Fe/Co/Ni-DACs located on the surface of Ti_2CO_2.

(B) Adsorption energies of different DACs@Ti_2CO_2 and neighbored oxygen vacancies in 4 × 4 supercell structures.

(C) Tensile/compression stress-strain curves and the relationship between reaction energy and strain magnitude.

(D) The ORR performance change with various applied strain for DACs system. Reproduced with permission from.[67] Copyright 2021 Wiley-VCH.

(E) The linear relationship between DFT calculated ΔG_{OH} and ML fitted ΔG_{OH}. Reproduced with permission from.[72] Copyright 2022 American Chemical Society.

(F) Color-coded map of adsorption energy vs. element's composition for PdCuZnTi.

(G) Schematic representation of $Pt_{0.5}Ni_{0.5}$ composition and partially and fully disordered probability distribution of the energies. Reproduced with permission from[73] copyright 2019 The Royal Society of Chemistry.

found that the structural disorder in MXene can be well defined by microstrain, which can calculated as Equation 19:[67]

$$\text{Microstrain} = f(\%M) + D^{*}SD \qquad \text{(Equation 19)}$$

The $f(\%M)$ is sum of bulk chemical disorder (obtained by DFT calculations and experiments) and surface defectiveness (SD), weighted by the surface-to-volume ratio (D).[71] The microstrain induced by dopant atoms is the descriptor to describe the structure fluctuation stability and catalytic activity (Figures 12A–12D).

Structural stability is a performance criterion of OER/ORR activity.[74] Saidi's research group calculated the *OH adsorption energy on the surface of PdAuAgTi series alloys with lower computational time and higher accuracy.[72] They found that substitutions of Au and Ag with Cu and Zn can produce better ORR catalysts. The thermodynamic stability of the alloy can be gauged by inspecting atomic radius difference between various metal elements (δ_r), the mixed entropy (ΔS_{mix}), and the mixed enthalpy (ΔH_{mix}). Those three parameters have great advantages for predicting the stability of the test system at different temperatures (Figures 12E and 12F).

Compound descriptors

For bulk electrocatalysts, the compound descriptor is complicated and mainly correlated with frontier electronic state which is near Fermi level. Li and coworkers explored the OER/ORR performance of

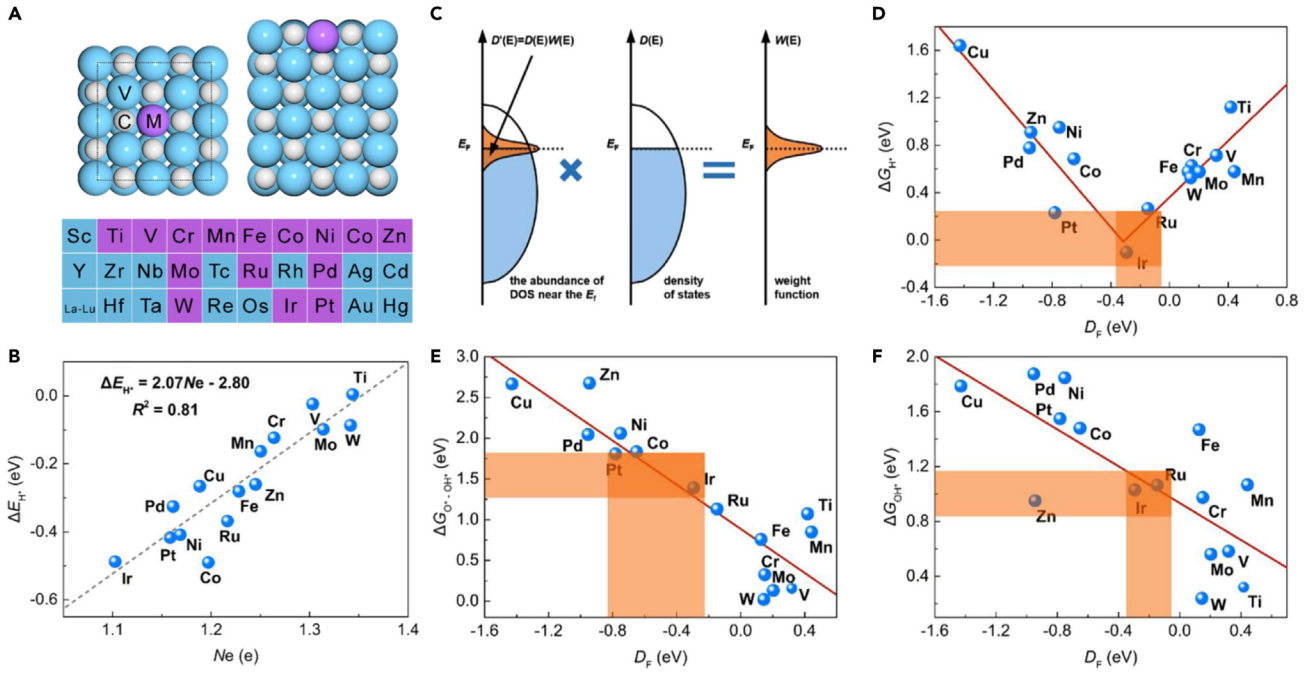

Figure 13. The atomic structure and compound descriptor-controlled performance

(A) The atomic models of TM-doped VC with (001) lattice plane exposed.

(B) The scaling linear of ΔE_H versus calculated electrons of C atom gains.

(C) Schematic plot of the abundance of DOS*(D′(E)=D(E)W(E))* defined as DOS and weight function multiplied near the Fermi level, the derivative of the Fermi-Dirac function is used as the weight function.

(D–F) The relationship between the adsorbed Gibbs free energy including ΔG_H, ΔG_O - ΔG_{OH} and ΔG_{OH} and corresponding Fermi-abundance for the TM-doped VC systems. Reproduced with permission from[75] copyright 2021 American Chemical Society.

various metal-doped vanadium carbide (VC) crystal with exposed (001) lattice plane on the basis of DFT theory.[75] The TMs were doped in VC to modulate the binding strength of key intermediates according to the change of chemical coordinated environment and corresponding electronic states. In these TMs-doped VC catalysts, the *d*-band center theory is not proper to describe the performance change due to every electronic state not presenting similar contributions to the bonding strength between adsorbates and catalyst surface. Although the entire frontier electronic band on the catalyst surface is active, the contribution also relates to the distance from their energy levels to the Fermi level. Thus, they introduced the fermi-abundance model to describe the catalytic activity of oxygen redox electrocatalysts on TM doped VC surfaces (Figure 13). The Fermi-abundance (D_F) is defined as Equation 20:

$$D_F = \frac{\int_{-\infty}^{+\infty} ED(E)W(E)dE}{\int_{-\infty}^{+\infty} D(E)W(E)dE} = \frac{\int_{-\infty}^{+\infty} ED'(E)dE}{\int_{-\infty}^{+\infty} D'(E)dE} \quad \text{(Equation 20)}$$

where $D'(E) = D(E)W(E)$ and $W(E)$ is the weight function ($W(E) = -f_T'(E - E_F)$) with the prime (′) representing the derivative.

$f_T(E - E_F)$ is the Fermi−Dirac distribution function and is calculated by:

$$f_T(E - E_F) = \frac{1}{\exp[(E - E_F)/kT] + 1} \quad \text{(Equation 21)}$$

where kT (0.1–1 eV) is the nominal electron temperature. The spreading of $W(E)$ can be adjusted by kT.

CONCLUSIONS AND OUTLOOK

Taking advantages of high-throughput computing and machine learning methods, the structure-activity relation can be studied from a wide range of degrees of freedom and descriptors can be effectively extracted from the atomic microscale, cluster mesoscale, and bulk macroscale catalysts. However, the feature engineering

toward constructing multiscale descriptors for prediction of novel catalysts remain a big challenge. Much more effort should be taken to the multiscale research and propose descriptors that link the overpotential with the structure and properties of catalysts for OER/ORR. Several important issues deserve exploration.

(1) The performance of electrocatalysts for OER/ORR can be affected by various factors such as defects, solvation effect, and surface coverage. The single-component descriptor cannot effectively evaluate the activity trend for all catalysts. Developing descriptors containing multi-factors is indeed necessary to describe the structure-performance relationship.

(2) From the atomic scale, the activity of OER/ORR electrocatalysts is determined by the geometrical and electronic structures of active sites, while it is also influenced by flux of solvents and electrical field from the macroscale. Seeking cross-scale descriptors that contain the experimental and test environmental feature parameters is directional to enhance the prediction accuracy of novel electrocatalysts.

(3) The OER and ORR are complicated electrochemical processes, including dynamic proton-electron transfer and dynamic evolution of active sites during reactions. The current descriptors are mainly based on the static electronic structure and geometric structure. More attention should be paid to capture the dynamic feature descriptors of electrocatalysis.

ACKNOWLEDGMENTS

This work was financially supported by the National Natural Science Foundation of China (52203303, 52220105010, M-0755), the Natural Science Foundation of Guangdong Province (2022A1515010076), the Natural Science Foundation of Shandong Province (ZR2020ZD35), the SIAT Innovation Program for Excellent Young Researchers (E2G017), and the CAS president's international fellowship initiative grant (2022 VEA0011, 2022VEA0016, 2022VEA0017). The Shenzhen Science and Technology Program (SGDX2021 1123151002003).

AUTHOR CONTRIBUTIONS

C. P., C.Y. Z., and D.F. X. supervised the preparation of this review article. D.T. Z. contributed to the most of the writing and Qi. Z. contributed to some content and figures. Z. L. and G.L. Z. revised the manuscript. D. K. and S. K. revised and finalized the manuscript. All author approved the final version of the manuscript.

DECLARATION OF INTERESTS

The authors declare no conflict of interest.

REFERENCES

1. Fu, M., Ma, X., Zhao, K., Li, X., and Su, D. (2021). High-entropy materials for energy-related applications. iScience *24*, 102177. https://doi.org/10.1016/j.isci.2021.102177.

2. Wang, K., Pei, P., Zuo, Y., Wei, M., Wang, H., Zhang, P., Chen, Z., and Shang, N. (2022). Magnetic zinc-air batteries for storing wind and solar energy. iScience *25*, 103837. https://doi.org/10.1016/j.isci.2022.103837.

3. Tian, Y., Wu, Z., Li, M., Sun, Q., Chen, H., Yuan, D., Deng, D., Johannessen, B., Wang, Y., Zhong, Y., et al. (2022). Atomic modulation and structure design of Fe−N_4 modified hollow carbon fibers with encapsulated Ni nanoparticles for rechargeable Zn–air batteries. Adv. Funct. Mater. *32*, 2209273. https://doi.org/10.1002/adfm.202209273.

4. Taylor, H.S. (1925). A theory of the catalytic surface. Proc. R. Soc. Lond. A *108*, 105–111. https://doi.org/10.1098/rspa.1925.0061.

5. Taylor, H.S. (1926). Fourth report of the committee on contact catalysis. J. Phys. Chem. *30*, 145–171.

6. Taylor, H.S. (1930). The activation energy of adsorption processes. J. Am. Chem. Soc. *52*, 5298–5299. https://doi.org/10.1021/ja01375a509.

7. Nørskov, J.K., Rossmeisl, J., Logadottir, A., Lindqvist, L., Kitchin, J.R., Bligaard, T., and Jónsson, H. (2004). Origin of the overpotential for oxygen reduction at a fuel-cell cathode. J. Phys. Chem. B *108*, 17886–17892. https://doi.org/10.1021/jp047349j.

8. Man, I.C., Su, H.Y., Calle-Vallejo, F., Hansen, H.A., Martínez, J.I., Inoglu, N.G., Kitchin, J., Jaramillo, T.F., Nørskov, J.K., and Rossmeisl, J. (2011). Universality in oxygen evolution electrocatalysis on oxide surfaces. ChemCatChem *3*, 1159–1165. https://doi.org/10.1002/cctc.201000397.

9. Govindarajan, N., García-Lastra, J.M., Meijer, E.J., and Calle-Vallejo, F. (2018). Does the breaking of adsorption-energy scaling relations guarantee enhanced electrocatalysis? Curr. Opin. Electrochem. *8*, 110–117. https://doi.org/10.1016/j.coelec.2018.03.025.

10. Li, J. (2022). Oxygen evolution reaction in energy conversion and storage: design strategies under and beyond the energy scaling relationship. Nano-Micro Lett. *14*, 112. https://doi.org/10.1007/s40820-022-00857-x.

11. Yang, X.F., Wang, A., Qiao, B., Li, J., Liu, J., and Zhang, T. (2013). Single-atom catalysts: a new Frontier in heterogeneous catalysis. Acc. Chem. Res. *46*, 1740–1748.

12. Ying, Y., Fan, K., Luo, X., Qiao, J., and Huang, H. (2021). Unravelling the origin of bifunctional OER/ORR activity for single-atom catalysts supported on C_2N by DFT and machine learning. J. Mater. Chem. *9*, 16860–16867. https://doi.org/10.1039/d1ta04256d.

13. Liu, J., Luo, W., Wang, L., Zhang, J., Fu, X.Z., and Luo, J.L. (2022). Toward excellence of electrocatalyst design by emerging descriptor-oriented machine learning. Adv. Funct. Mater. *32*, 2110748. https://doi.org/10.1002/adfm.202110748.

14. Lin, S., Xu, H., Wang, Y., Zeng, X.C., and Chen, Z. (2020). Directly predicting limiting potentials from easily obtainable physical properties of graphene-supported single-atom electrocatalysts by machine learning. J. Mater. Chem. *8*, 5663–5670. https://doi.org/10.1039/c9ta13404b.

15. Agyeman, D.A., Zheng, Y., Lee, T.-H., Park, M., Tamakloe, W., Lee, G.-H., Jang, H.W., Cho, K., and Kang, Y.-M. (2020). Synergistic catalysis of the lattice oxygen and transition metal facilitating ORR and OER in perovskite catalysts for Li–O_2 batteries. ACS Catal. *11*, 424–434. https://doi.org/10.1021/acscatal.0c02608.

16. Calle-Vallejo, F., Díaz-Morales, O.A., Kolb, M.J., and Koper, M.T.M. (2015). Why is bulk thermochemistry a good descriptor for the electrocatalytic activity of transition metal oxides? ACS Catal. *5*, 869–873. https://doi.org/10.1021/cs5016657.

17. Ha, M., Kim, D.Y., Umer, M., Gladkikh, V., Myung, C.W., and Kim, K.S. (2021). Tuning metal single atoms embedded in N_xC_y moieties toward high-performance electrocatalysis. Energy Environ. Sci. *14*, 3455–3468. https://doi.org/10.1039/d1ee00154j.

18. Liu, J., Xiao, J., Luo, B., Tian, E., and Waterhouse, G.I. (2022). Central metal and ligand effects on oxygen electrocatalysis over 3*d* transition metal single-atom catalysts: a theoretical investigation. Chem. Eng. J. *427*, 132038. https://doi.org/10.1016/j.cej.2021.132038.

19. Liu, K., Fu, J., Lin, Y., Luo, T., Ni, G., Li, H., Lin, Z., and Liu, M. (2022). Insights into the activity of single-atom Fe-N-C catalysts for oxygen reduction reaction. Nat. Commun. *13*, 2075. https://doi.org/10.1038/s41467-022-29797-1.

20. Miyahara, Y., Fukutsuka, T., Abe, T., and Miyazaki, K. (2020). Dual-site catalysis of Fe-incorporated oxychlorides as oxygen evolution electrocatalysts. Chem. Mater. *32*, 8195–8202. https://doi.org/10.1021/acs.chemmater.0c01674.

21. He, F., Liu, Y., Cai, Q., and Zhao, J. (2020). Size-dependent electrocatalytic activity of ORR/OER on palladium nanoclusters anchored on defective MoS_2 monolayers. New J. Chem. *44*, 16135–16143. https://doi.org/10.1039/d0nj03645e.

22. Sun, F., Yang, C., Qu, Z., Zhou, W., Ding, Y., Gao, J., Zhao, G., Xing, D., and Lu, Y. (2021). Inexpensive activated coke electrocatalyst for high-efficiency hydrogen peroxide production: coupling effects of amorphous carbon cluster and oxygen dopant. Appl. Catal., B *286*, 119860. https://doi.org/10.1016/j.apcatb.2020.119860.

23. Jin, Z., Lyu, J., Zhao, Y.-L., Li, H., Chen, Z., Lin, X., Xie, G., Liu, X., Kai, J.-J., and Qiu, H.-J. (2021). Top–down synthesis of noble metal particles on high-entropy oxide supports for electrocatalysis. Chem. Mater. *33*, 1771–1780. https://doi.org/10.1021/acs.chemmater.0c04695.

24. Huang, Z.-F., Wang, J., Peng, Y., Jung, C.-Y., Fisher, A., and Wang, X. (2017). Design of efficient bifunctional oxygen reduction/evolution electrocatalyst: recent advances and perspectives. Adv. Energy Mater. *7*, 1700544. https://doi.org/10.1002/aenm.201700544.

25. Dong, C., Gao, Z., Li, Y., Peng, M., Wang, M., Xu, Y., Li, C., Xu, M., Deng, Y., Qin, X., et al. (2022). Fully exposed palladium cluster catalysts enable hydrogen production from nitrogen heterocycles. Nat. Catal. *5*, 485–493. https://doi.org/10.1038/s41929-022-00769-4.

26. Arikado, T., Iwakura, C., and Tamura, H. (1978). Some oxide catalysts for the anodic evolution of chlorine: reaction mechanism and catalytic activity. Electrochim. Acta *23*, 9–15.

27. Kim, S.-h., Kang, Y., and Ham, H.C. (2021). First-principles study of Pt-based bifunctional oxygen evolution & reduction electrocatalyst: interplay of strain and ligand effects. Energies *14*, 7814. https://doi.org/10.3390/en14227814.

28. Hill, C.M., Mendoza-Cortes, J.L., Velázquez, J.M., and Whittaker-Brooks, L. (2022). Multi-dimensional designer catalysts for negative emissions science (nes): bridging the gap between synthesis, simulations, and analysis. iScience *25*, 103700. https://doi.org/10.1016/j.isci.2021.103700.

29. Wang, W., Yang, Y., Zhao, Y., Wang, S., Ai, X., Fang, J., and Liu, Y. (2021). Multi-scale regulation in s, n co-incorporated carbon encapsulated Fe-doped Co_9S_8 achieving efficient water oxidation with low overpotential. Nano Res. *15*, 872–880. https://doi.org/10.1007/s12274-021-3568-8.

30. Exner, K.S., and Over, H. (2017). Kinetics of electrocatalytic reactions from first-principles: a critical comparison with the ab initio thermodynamics approach. Acc. Chem. Res. *50*, 1240–1247. https://doi.org/10.1021/acs.accounts.7b00077.

31. Chattot, R., Le Bacq, O., Beermann, V., Kühl, S., Herranz, J., Henning, S., Kühn, L., Asset, T., Guétaz, L., Renou, G., et al. (2018). Surface distortion as a unifying concept and descriptor in oxygen reduction reaction electrocatalysis. Nat. Mater. *17*, 827–833. https://doi.org/10.1038/s41563-018-0133-2.

32. Baeumer, C., Li, J., Lu, Q., Liang, A.Y.L., Jin, L., Martins, H.P., Duchoň, T., Glöß, M., Gericke, S.M., Wohlgemuth, M.A., et al. (2021). Tuning electrochemically driven surface transformation in atomically flat $LaNiO_3$ thin films for enhanced water electrolysis. Nat. Mater. *20*, 674–682. https://doi.org/10.1038/s41563-020-00877-1.

33. Rittiruam, M., Somdee, S., Buapin, P., Aumnongpho, N., Kerdprasit, N., Saelee, T., Kheawhom, S., Chotigkrai, N., Praserthdam, S., and Praserthdam, P. (2021). On the deactivation mechanisms of MnO_2 electrocatalyst during operation in rechargeable zinc-air batteries studied via density functional theory. J. Alloys Compd. *869*, 159280. https://doi.org/10.1016/j.jallcom.2021.159280.

34. Hale, W., and Choudhury, P. (2022). Thermodynamic stability and intrinsic activity of $La_{1-x}Sr_xMnO_3$ (LSM) as an efficient bifunctional OER/ORR electrocatalysts: a theoretical study. Catalysts *12*, 260. https://doi.org/10.3390/catal12030260.

35. Wei, C., Feng, Z., Scherer, G.G., Barber, J., Shao-Horn, Y., and Xu, Z.J. (2017). Cations in octahedral sites: a descriptor for oxygen electrocatalysis on transition-metal spinels. Adv. Mater. *29*, 1606800. https://doi.org/10.1002/adma.201606800.

36. Huang, Z.-F., Lin, B.Q., Torsha, T.T., Dilshad, S., Yang, D.S., Xiao, J., Wang, C., Xu, Z.J., and Wang, X. (2019). Chemical and structural origin of lattice oxygen oxidation in Co–Zn oxyhydroxide oxygen evolution electrocatalysts. Nat. Energy *32*, 329–337. https://doi.org/10.1038/s41560-019-0355-9.

37. Rong, X., Parolin, J., and Kolpak, A.M. (2016). A fundamental relationship between reaction mechanism and stability in metal oxide catalysts for oxygen evolution. ACS Catal. *6*, 1153–1158. https://doi.org/10.1021/acscatal.5b02432.

38. Liu, X., Zhang, G., Wang, L., and Fu, H. (2021). Structural design strategy and active site regulation of high-efficient bifunctional oxygen reaction electrocatalysts for Zn-air battery. Small *17*, e2006766. https://doi.org/10.1002/smll.202006766.

39. Kulkarni, A., Siahrostami, S., Patel, A., and Nørskov, J.K. (2018). Understanding catalytic activity trends in the oxygen reduction reaction. Chem. Rev. *118*, 2302–2312. https://doi.org/10.1021/acs.chemrev.7b00488.

40. Liang, Q., Brocks, G., and Bieberle-Hütter, A. (2021). Oxygen evolution reaction (OER) mechanism under alkaline and acidic conditions. J. Phys. Energy *3*, 026001. https://doi.org/10.1088/2515-7655/abdc85.

41. Liu, J., Liu, H., Chen, H., Du, X., Zhang, B., Hong, Z., Sun, S., and Wang, W. (2020). Progress and challenges toward the rational design of oxygen electrocatalysts based on a descriptor approach. Adv. Sci. *7*, 1901614. https://doi.org/10.1002/advs.201901614.

42. Zhong, W., Qiu, Y., Shen, H., Wang, X., Yuan, J., Jia, C., Bi, S., and Jiang, J. (2021). Electronic spin moment as a catalytic descriptor for Fe single-atom catalysts supported on C_2N. J. Am. Chem. Soc. *143*, 4405–4413. https://doi.org/10.1021/jacs.1c00889.

43. Di Liberto, G., Cipriano, L.A., and Pacchioni, G. (2022). Universal principles for the rational design of single atom electrocatalysts? Handle with care. ACS Catal. *12*, 5846–5856. https://doi.org/10.1021/acscatal.2c01011.

44. Yin, C., Tang, H., Li, K., Yuan, Y., and Wu, Z. (2018). Theoretical insight into the catalytic activities of oxygen reduction reaction on transition metal–N_4 doped graphene. New J. Chem. *42*, 9620–9625. https://doi.org/10.1039/c8nj01593g.

45. Zhou, X., Gao, J., Hu, Y., Jin, Z., Hu, K., Reddy, K.M., Yuan, Q., Lin, X., and Qiu, H.J. (2022). Theoretically revealed and experimentally demonstrated synergistic electronic interaction of cofe dual-metal sites on

n-doped carbon for boosting both oxygen reduction and evolution reactions. Nano Lett. *22*, 3392–3399. https://doi.org/10.1021/acs.nanolett.2c00658.

46. Hammer, B., and Nørskov, J. (1995). Electronic factors determining the reactivity of metal surfaces. Surf. Sci. *343*, 211–220.

47. Jiao, S., Fu, X., and Huang, H. (2021). Descriptors for the evaluation of electrocatalytic reactions: *D*-band theory and beyond. Adv. Funct. Mater. *32*, 2107651. https://doi.org/10.1002/adfm.202107651.

48. Wan, X., Yu, W., Niu, H., Wang, X., Zhang, Z., and Guo, Y. (2022). Revealing the oxygen reduction/evolution reaction activity origin of carbon-nitride-related single-atom catalysts: quantum chemistry in artificial intelligence. Chem. Eng. J. *440*, 135946. https://doi.org/10.1016/j.cej.2022.135946.

49. Liu, X., Zhang, Y., Wang, W., Chen, Y., Xiao, W., Liu, T., Zhong, Z., Luo, Z., Ding, Z., and Zhang, Z. (2022). Transition metal and n doping on AlP monolayers for bifunctional oxygen electrocatalysts: density functional theory study assisted by machine learning description. ACS Appl. Mater. Interfaces *14*, 1249–1259. https://doi.org/10.1021/acsami.1c22309.

50. Jing, T., Liang, D., Deng, M., Cai, S., and Qi, X. (2021). Density functional theory studies of heteroatom-doped graphene-like GaN monolayers as electrocatalysts for oxygen evolution and reduction. ACS Appl. Nano Mater. *4*, 7125–7133. https://doi.org/10.1021/acsanm.1c01119.

51. Wu, L., Guo, T., and Li, T. (2022). Data-driven high-throughput rational design of double-atom catalysts for oxygen evolution and reduction. Adv. Funct. Mater. *32*, 2203439. https://doi.org/10.1002/adfm.202203439.

52. Zhao, Z., Li, M., Zhang, L., Dai, L., and Xia, Z. (2015). Design principles for heteroatom-doped carbon nanomaterials as highly efficient catalysts for fuel cells and metal-air batteries. Adv. Mater. *27*, 6834–6840. https://doi.org/10.1002/adma.201503211.

53. Zhang, L., Guo, X., Zhang, S., and Huang, S. (2022). Building up the "genome" of bi-atom catalysts toward efficient HER/OER/ORR. J. Mater. Chem. *10*, 11600–11612. https://doi.org/10.1039/d2ta02050e.

54. Vázquez-Lizardi, G.A., Ruiz-Casanova, L.A., Cruz-Sánchez, R.M., and Santana, J.A. (2021). Simulation of metal-supported metal-nanoislands: a comparison of DFT methods. Surf. Sci. *712*, 121889. https://doi.org/10.1016/j.susc.2021.121889.

55. Zhou, Y., Gao, G., Chu, W., and Wang, L.W. (2020). Computational screening of transition metal-doped phthalocyanine monolayers for oxygen evolution and reduction. Nanoscale Adv. *2*, 710–716. https://doi.org/10.1039/c9na00648f.

56. Zhao, X., Liu, X., Huang, B., Wang, P., and Pei, Y. (2019). Hydroxyl group modification improves the electrocatalytic ORR and OER activity of graphene supported single and bi-metal atomic catalysts (Ni, Co, and Fe). J. Mater. Chem. *7*, 24583–24593. https://doi.org/10.1039/c9ta08661g.

57. Anand, R., Nissimagoudar, A.S., Umer, M., Ha, M., Zafari, M., Umer, S., Lee, G., and Kim, K.S. (2021). Late transition metal doped mxenes showing superb bifunctional electrocatalytic activities for water splitting via distinctive mechanistic pathways. Adv. Energy Mater. *11*, 2102388. https://doi.org/10.1002/aenm.202102388.

58. Chattot, R., Bordet, P., Martens, I., Drnec, J., Dubau, L., and Maillard, F. (2020). Building practical descriptors for defect engineering of electrocatalytic materials. ACS Catal. *10*, 9046–9056. https://doi.org/10.1021/acscatal.0c02144.

59. Deshpande, S., Kitchin, J.R., and Viswanathan, V. (2016). Quantifying uncertainty in activity volcano relationships for oxygen reduction reaction. ACS Catal. *6*, 5251–5259. https://doi.org/10.1021/acscatal.6b00509.

60. Radinger, H., Trouillet, V., Bauer, F., and Scheiba, F. (2022). Work function describes the electrocatalytic activity of graphite for vanadium oxidation. ACS Catal. *12*, 6007–6015. https://doi.org/10.1021/acscatal.2c00334.

61. Sun, F., Tang, Q., and Jiang, D.E. (2022). Theoretical advances in understanding and designing the active sites for hydrogen evolution reaction. ACS Catal. *12*, 8404–8433. https://doi.org/10.1021/acscatal.2c02081.

62. Lu, S., Huynh, H.L., Lou, F., Guo, K., and Yu, Z. (2021). Single transition metal atom embedded antimonene monolayers as efficient trifunctional electrocatalysts for the HER, OER and ORR: a density functional theory study. Nanoscale *13*, 12885–12895. https://doi.org/10.1039/d1nr02235k.

63. Ma, J., Zhi, Q., Gong, L., Shen, Y., Sun, D., Guo, Y., Zhang, L., and Xia, Z. (2020). A universal descriptor based on pz-orbitals for the catalytic activity of multi-doped carbon bifunctional catalysts for oxygen reduction and evolution. Nanoscale *12*, 19375–19382. https://doi.org/10.1039/d0nr03521a.

64. Kirsanova, M.A., Okatenko, V.D., Aksyonov, D.A., Forslund, R.P., Mefford, J.T., Stevenson, K.J., and Abakumov, A. (2019). Bifunctional OER/ORR catalytic activity in the tetrahedral $YBaCo_4O_{7.3}$ oxide. J. Mater. Chem. *7*, 330–341. https://doi.org/10.1039/c8ta09862j.

65. Xu, W., Andersen, M., and Reuter, K. (2020). Data-driven descriptor engineering and refined scaling relations for predicting transition metal oxide reactivity. ACS Catal. *11*, 734–742. https://doi.org/10.1021/acscatal.0c04170.

66. Lee, H., Gwon, O., Choi, K., Zhang, L., Zhou, J., Park, J., Yoo, J.-W., Wang, J.Q., Lee, J.H., and Kim, G. (2020). Enhancing bifunctional electrocatalytic activities via metal *d*-band center lift induced by oxygen vacancy on the subsurface of perovskites. ACS Catal. *10*, 4664–4670. https://doi.org/10.1021/acscatal.0c01104.

67. Wei, B., Fu, Z., Legut, D., Germann, T.C., Du, S., Zhang, H., Francisco, J.S., and Zhang, R. (2021). Rational design of highly stable and active mxene-based bifunctional ORR/OER double-atom catalysts. Adv. Mater. *33*, e2102595. https://doi.org/10.1002/adma.202102595.

68. Xie, J., Wang, Y., Chen, G., and Chen, D. (2022). Compositional and morphology optimization to boost the bifunctionality of perovskite oxygen electrocatalysts. ACS Appl. Energy Mater. *5*, 7420–7431. https://doi.org/10.1021/acsaem.2c00927.

69. Alkhalifah, M.A., Howchen, B., Staddon, J., Celorrio, V., Tiwari, D., and Fermin, D.J. (2022). Correlating orbital composition and activity of $LaMn_xNi_{1-x}O_3$ nanostructures toward oxygen electrocatalysis. J. Am. Chem. Soc. *144*, 4439–4447. https://doi.org/10.1021/jacs.1c11757.

70. Zhao, Z., D'Souza, J., Chen, F., and Xia, Z. (2018). Rational design of efficient transition metal core-shell electrocatalysts for oxygen reduction and evolution reactions. RSC Adv. *9*, 536–542. https://doi.org/10.1039/c8ra09122f.

71. Montejano-Carrizales, J.M., and Morán-López, J. (1992). Geometrical characteristics of compact nanoclusters. Nanostruct. Mater. *1*, 397–409.

72. Saidi, W.A. (2022). Optimizing the catalytic activity of Pd-based multinary alloys toward oxygen reduction reaction. J. Phys. Chem. Lett. *13*, 1042–1048. https://doi.org/10.1021/acs.jpclett.1c04128.

73. Botha, L.M., Santos-Carballal, D., Terranova, U., Quesne, M.G., Ungerer, M.J., van Sittert, C.G.C.E., and de Leeuw, N.H. (2019). Mixing thermodynamics and electronic structure of the $Pt_{1-x}Ni_x$ ($0 \leq x \leq 1$) bimetallic alloy. RSC Adv. *9*, 16948–16954. https://doi.org/10.1039/c9ra02320h.

74. Zhang, H., Liu, W., Cao, D., and Cheng, D. (2022). Carbon-based material-supported single-atom catalysts for energy conversion. iScience *25*, 104367. https://doi.org/10.1016/j.isci.2022.104367.

75. Zhao, R., Yang, C., Zhang, Q., Xiang, H., Li, Y., and Li, X. (2021). Transition metal-promoted VC(001) for overall water splitting and oxygen reduction. J. Phys. Chem. C *125*, 14607–14615. https://doi.org/10.1021/acs.jpcc.1c02020.